NAVAL POSTGRADUATE SCHOOL

MONTEREY, CALIFORNIA

THESIS

FLOW FIELD SURVEYS IN A TRANSONIC COMPRESSOR RIG

by

Christopher W. Rose

June 2006

Thesis Advisor:	Garth V. Hobson
Second Reader:	Anthony J. Gannon

THIS PAGE INTENTIONALLY LEFT BLANK

REPORT DOCUMENTATION PAGE		Form Approved OMB No. 0704-0188

1. AGENCY USE ONLY *(Leave blank)*	2. REPORT DATE	3. REPORT TYPE AND DATES COVERED
	June 2006	Master's Thesis

4. TITLE AND SUBTITLE Flow Field Survey in a Transonic Compressor Rig	**5. FUNDING NUMBERS**
6. AUTHOR(S) Christopher W. Rose	
7. PERFORMING ORGANIZATION NAME(S) AND ADDRESS(ES) Naval Postgraduate School Monterey, CA 93943-5000	**8. PERFORMING ORGANIZATION REPORT NUMBER**
9. SPONSORING /MONITORING AGENCY NAME(S) AND ADDRESS(ES) N/A	**10. SPONSORING/MONITORING AGENCY REPORT NUMBER**
11. SUPPLEMENTARY NOTES The views expressed in this thesis are those of the author and do not reflect the official policy or position of the Department of Defense or the U.S. Government.	
12a. DISTRIBUTION / AVAILABILITY STATEMENT Approved for public release; distribution is unlimited	**12b. DISTRIBUTION CODE**

13. ABSTRACT (maximum 200 words)

As the Navy prepares to transition to F-35C Joint Strike Fighter the need to understand "pop stalls" caused by steam leakage in catapult systems is of concern. "Pop stalls" caused by steam ingestion through the aircraft engine result in a loss of power and possible engine stall. The F-35C is a single engine aircraft and therefore the probability of a "pop stall" resulting in the loss of the aircraft is increased. Investigation of this phenomenon is currently being examined at the Turbopropulsion Laboratory by means of a transonic compressor rotor. The present study utilizes both three and five-hole probes to survey the flow field upstream and downstream of the rotor to examine compressor stability. A new compressor performance map was defined and a validation of previous steam ingestion was performed.

14. SUBJECT TERMS Compressor, Transonic, Steam Ingestion, Inlet Distortion, Turbomachinery, Pop Stall, Rotor			**15. NUMBER OF PAGES** 69
			16. PRICE CODE
17. SECURITY CLASSIFICATION OF REPORT Unclassified	**18. SECURITY CLASSIFICATION OF THIS PAGE** Unclassified	**19. SECURITY CLASSIFICATION OF ABSTRACT** Unclassified	**20. LIMITATION OF ABSTRACT** UL

NSN 7540-01-280-5500 Standard Form 298 (Rev. 2-89)
Prescribed by ANSI Std. 239-18

THIS PAGE INTENTIONALLY LEFT BLANK

Approved for public release; distribution is unlimited

FLOW FIELD SURVEY IN A TRANSONIC COMPRESSOR RIG

Christopher W. Rose
Ensign, United States Navy
B.S., United States Naval Academy, 2006

Submitted in partial fulfillment of the
requirements for the degree of

MASTER OF SCIENCE IN MECHANICAL ENGINEERING

from the

NAVAL POSTGRADUATE SCHOOL
June 2006

Author: Christopher Rose

Approved by: Garth V. Hobson
Thesis Advisor

Anthony J. Gannon
Second Reader

Anthony J. Healey
Chairman, Department of Mechanical and Astronautical Engineering

THIS PAGE INTENTIONALLY LEFT BLANK

ABSTRACT

As the Navy prepares to transition to F-35C Joint Strike Fighter the need to understand “pop stalls” caused by steam leakage in catapult systems is of concern. “Pop stalls” caused by steam ingestion through the aircraft engine result in a loss of power and possible engine stall. The F-35C is a single engine aircraft and therefore the probability of a “pop stall” resulting in the loss of the aircraft is increased. Investigation of this phenomenon is currently being examined at the Turbopropulsion Laboratory by means of a transonic compressor rotor. The present study utilizes both three and five-hole probes to survey the flow field upstream and downstream of the rotor to examine compressor stability. A new compressor performance map was defined and a validation of previous steam ingestion was performed.

THIS PAGE INTENTIONALLY LEFT BLANK

TABLE OF CONTENTS

LIST OF FIGURES

THIS PAGE INTENTIONALLY LEFT BLANK

LIST OF TABLES

THIS PAGE INTENTIONALLY LEFT BLANK

ACKNOWLEDGMENTS

I would like to thank everyone who aided me in completion of this project. The support from the entire Turbopropulsion Laboratory made this an enjoyable process and I could not have asked for a better environment in which to work than the one provided.

I would foremost like to thank Professor Garth Hobson for his guidance and help through the many adversities faced along the way. The support received from him through the tough times gave a feeling of reassurance that things would work themselves out in the end.

Special thanks to Rick Still and John Gibson for the hours spent troubleshooting all the problems that arose throughout this process. Their hard work along with sense of humor made the time spent at the lab pass quickly and always with a smile on my face.

I would finally like to thank all current and past students from the Turbopropulsion laboratory who aided in offering their lessons learned, guidance in procedures, and for making the laboratory an enjoyable place to work.

THIS PAGE INTENTIONALLY LEFT BLANK

I. INTRODUCTION

The F-35C Joint Strike Fighter (JSF) is a single engine fighter preparing to enter service in the United States Navy in the coming years. The aircraft will be powered by a single Pratt and Whitney F-135 engine and will be the first single engine airframe to be used in carrier operations in recent years. Studies performed on the F-18 at the Lakehurst Naval Air Engineering Station have shown the aircraft to be susceptible to "pop stalls" caused by steam ingestion during catapult launch which could cause a loss of power or total engine stall, shown in Figure 1. The F-18 utilizes two General Electric F404/414 engines which allow one engine to loose power during take-off without loss of the aircraft. Although the engines in the F-18 and F-35C are different, the JSF is susceptible to the same "pop stalls" caused by steam ingestion on launch. (Donelson, 2003)

Figure 1. F-18 Experiencing "pop stall" due to steam ingestion [From Ref 12]

The Turbopropulsion Laboratory (TPL) at the Naval Postgraduate School (NPS) is currently conducting studies to determine the effects of steam ingestion on a transonic compressor. Experimentations to further the understanding of the "pop stall" phenomena faced by United States Navy aircraft are the primary focus of the TPL. To evaluate

performance during steam-induced stall the TPL utilizes the rotor of the first stage of a transonic compressor. The low aspect ratio transonic compressor currently used at the TPL was designed by Nelson Sanger (1996) at the NASA Lewis Research Center using Computational Fluid Dynamics (CFD) modeling.

Previous studies of the compressor performed by Gannon, Hobson, and Shreeve have mapped compressor performance in the rotor only configuration. From this data, the Transonic Compressor Rig (TCR) performance characteristics were established at 70, 80, 90, and 100 percent design speeds. (Gannon, Hobson, and Shreeve, 2005)

Studies have continued to include flow-field surveys upstream and downstream of the rotor at varying design speeds and mass flow rates. Data were first obtained using a 3-hole pressure probe at 70, 80, 90 and 100 percent design speeds with mass flow rates at open throttle, peak efficiency, and near stall conditions. (Villescas, 2005) Follow-on work included measurements using a 5-hole pressure probe at similar design speeds and mass flow rates which allowed for the inlet pitch angle to be determined. (Brunner, 2005)

Recent changes to the inlet honeycomb have altered the performance characteristics of the TCR. Remapping the compressor performance was necessary to determine the new stall line of the compressor as well as peak efficiency mass flow rates. Previously taken steam ingestion induced stall tests (Payne, 2005) were repeated at 70 percent speed to also determine the change due to the inlet alterations. Upstream flow field surveys were performed at 70 and 90 percent at open throttle, peak efficiency, and near stall conditions. A downstream flow field survey was performed at 70 percent design speed at the previously mentioned throttle conditions.

II. EXPERIMENTAL TESTING FACILITY AND EQUIPMENT

The current research was conducted on the transonic compressor rig at the Turbopropulsion Laboratory (TPL) of the Naval Postgraduate School.

A. TRANSONIC COMPRESSOR RIG

The Transonic Compressor Rig (TCR) was designed by Professor Michael Vavra to test a transonic compressor stage. The TCR is driven by two opposed air turbine stages, supplied by an Allison Chalmers axial compressor. The test compressor was tested and detailed extensively by O'Brien (2000) and Papamarkos (2004). The TCR with inlet piping removed is shown in Figure 2.

Figure 2. TCR with inlet piping removed [From Ref. 12]

The transonic compressor rotor, shown in Figure 3, was part of a complete fan stage designed by Sanger using Computational Fluid Dynamic (CFD) techniques and was designed specifically for testing within the TCR. The rotor contains 22 blades and was machined from high strength aluminum (7075-T6) alloy. (Sanger, 1996) The current rotor utilizes a parabolic spinner which replaced the original conical spinner. (Gannon et al., 2005) The design parameters of the rotor are detailed in Table 1.

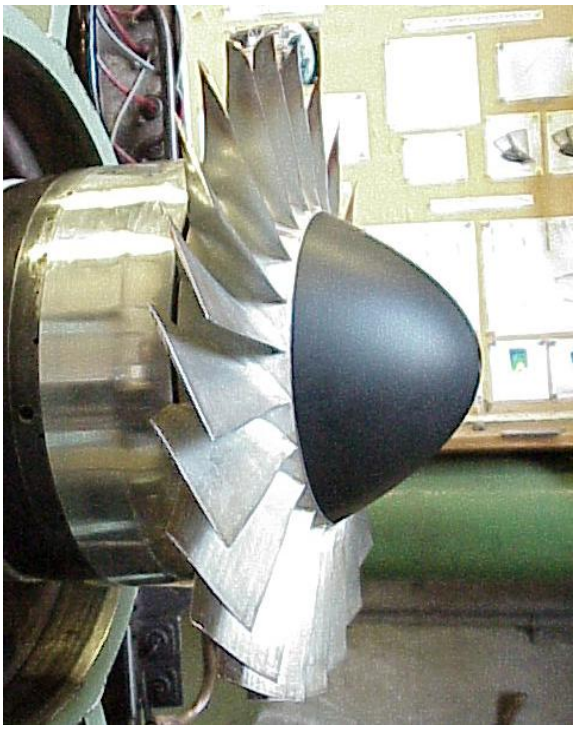

Figure 3. Sanger rotor [From Ref. 8]

Parameter	Value
Pressure Ratio	1.61
Tip Speed	33.02 m/s (1300 ft/s)
Design Speed	27085 rpm
Design Mass Flow	7.75 kg/s (17.05 lbs)
Specific Mass Flow	170.88 kg/s-m^2 (35 lbm/s-ft^2)
Specific Head Rise	0.246
Tip Inlet Relative Mach Number	1.28
Aspect Ratio	1.2
Hub/Tip Radius Ratio	0.51
Rotor Inlet Temp Ratio	28.2
Number of Rotor Blades	22
Tip Solidity	1.3
Outside Diameter	.2749m (11 inches)
Rotor Diffusion Factor- Tip	0.4
Rotor Diffusion Factor- Hub	0.47

Table 1. Sanger rotor design parameters [From Ref. 10]

The steel wall encapsulating the compressor was used to mount instrumentation for measurements. Four holes in the case wall were specifically drilled to accommodate a probe actuator for flow measurements and are shown in Figure 4. The gold band represents the location of the rotor, with holes one and two upstream of the rotor and holes three and four downstream of the rotor. Holes one and four were used to mount the actuator during the current project. Hole one was located approximately 11.15 cm (4.39 inches) upstream from the leading edge of the rotor and hole four was located approximately 5.49 cm (2.34 inches) downstream from the trailing edge of the rotor. (Villescas, 2005) A more detailed schematic of the case wall is shown in Appendix A.

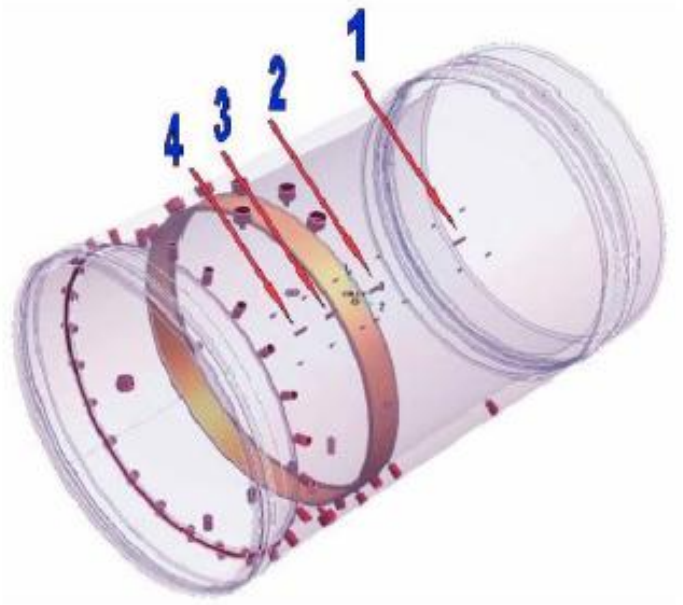

Figure 4. Case wall schematic illustrating probe mounting locations [From Ref.12]

Air was drawn in from the atmosphere through an inlet throttle valve and into a settling chamber. A 46 cm (18.11 inch) diameter, five-meter (16.4 foot) long inlet pipe connected the settling chamber to the test compressor. The pipe contained a nozzle, used for flow rate measurements, and a transition duct to the 27.94 cm (11 in) case wall.

Recent changes to the inlet of the transonic compressor rig have changed the flow characteristics within the system. The original hydraulic throttle was replaced with an

electric throttle and the three grates in the settling chamber were cleaned. A new honeycomb screen was installed made of type 304 stainless steel with .01 cm (.004 in) by 5.08 cm (2 in) hexagonal cells. A complete layout of the compressor rig, steam ingestion system, and probe sampling locations are shown in Figure 5.

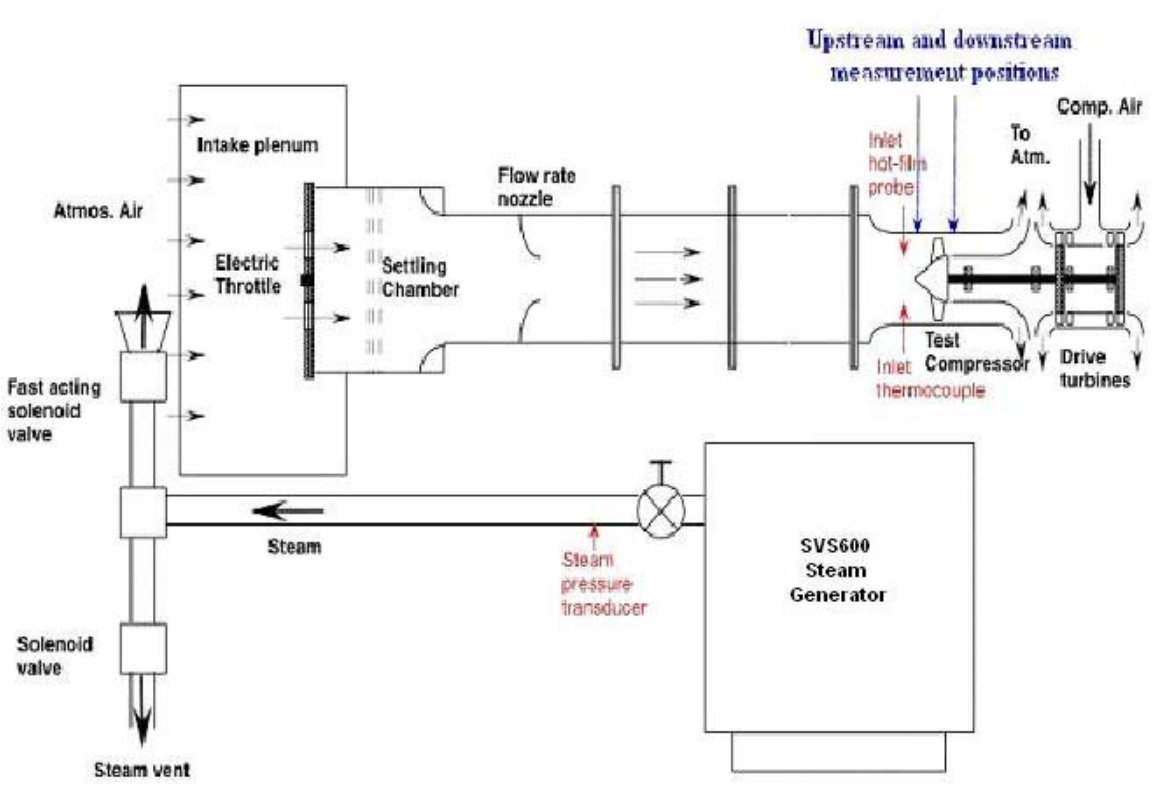

Figure 5. Compressor and steam ingestion system layout [From Ref. 8]

B. STEAM INGESTION SYSTEM

Steam was provided to the TCR by means of a Sussman model SVS600 steam generator. The SVS600 was located in a test cell adjacent to the TCR and contained a 612 kW boiler. The boiler was capable of providing steam at a Boiler Horsepower (BHP) rating of 62.4, corresponding to a steam supply of 1000 kPa (150 psig) or 1.4 kg/sec (30.1 lbs/sec) at 100˚C (212˚F). (Sussman, 2004)

Steam produced by the SVS600 was directed to the test rig inlet via a 7.62 cm (3 in) diameter pipe. Before entering the test cell, the steam passed through a manual shutoff valve and two fast acting, remote-operated solenoid valves to vent pipes and release

steam to the TCR intake as shown in Figure 6. Pressure transducers monitored the transient response of steam pressure. (Payne, 2005)

Figure 6. Steam pipe and intake plenum orientation [From Ref. 8]

THIS PAGE INTENTIONALLY LEFT BLANK

III. INSTRUMENTATION AND DATA ACQUISITION SYSTEM

A. FIVE-HOLE PROBE

A standard five-hole probe, as shown below in Figure 7 was the primary test probe for measurements in the current project.

Figure 7. Five-hole probe [From Ref. 2]

The layout of the pressure ports is presented in Figure 8.

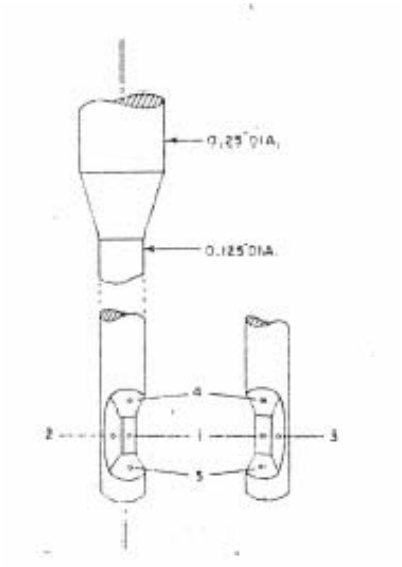

Figure 8. Five hole probe pressure port schematic [From Ref 1]

B. THREE-HOLE PROBE

To verify the affects of the new honeycomb screen on the airflow within the compressor, a three-hole cobra probe, shown in Figure 9, was also used. Data taken using the three-hole probe were then compared to measurements from Villescas who performed flow-field surveys both upstream and downstream of the rotor.

Figure 9. Three-hole cobra probe [From Ref 12]

The numbering of ports on the three-hole probe is shown in Figure 10.

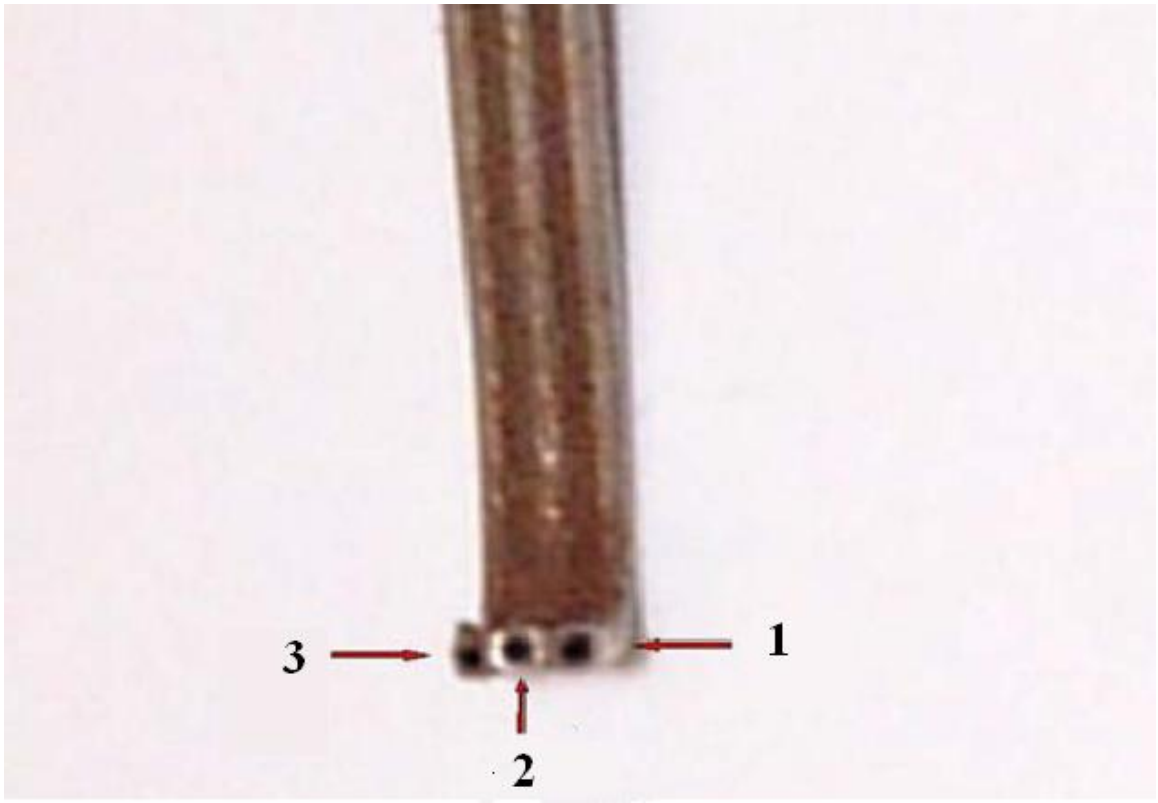

Figure 10. Three-hole probe numbering

C. PROBE ACTUATOR

The L.C. Smith probe actuator was driven by two electric motors which inserted, extracted, and rotated the probe during testing within the TCR. The probes were mounted into the L.C. Smith Probe actuator, which in turn was mounted on the case wall as shown in Figure 11. The setup of the probe actuator and PC control board were the same as described by Villescas (2005).

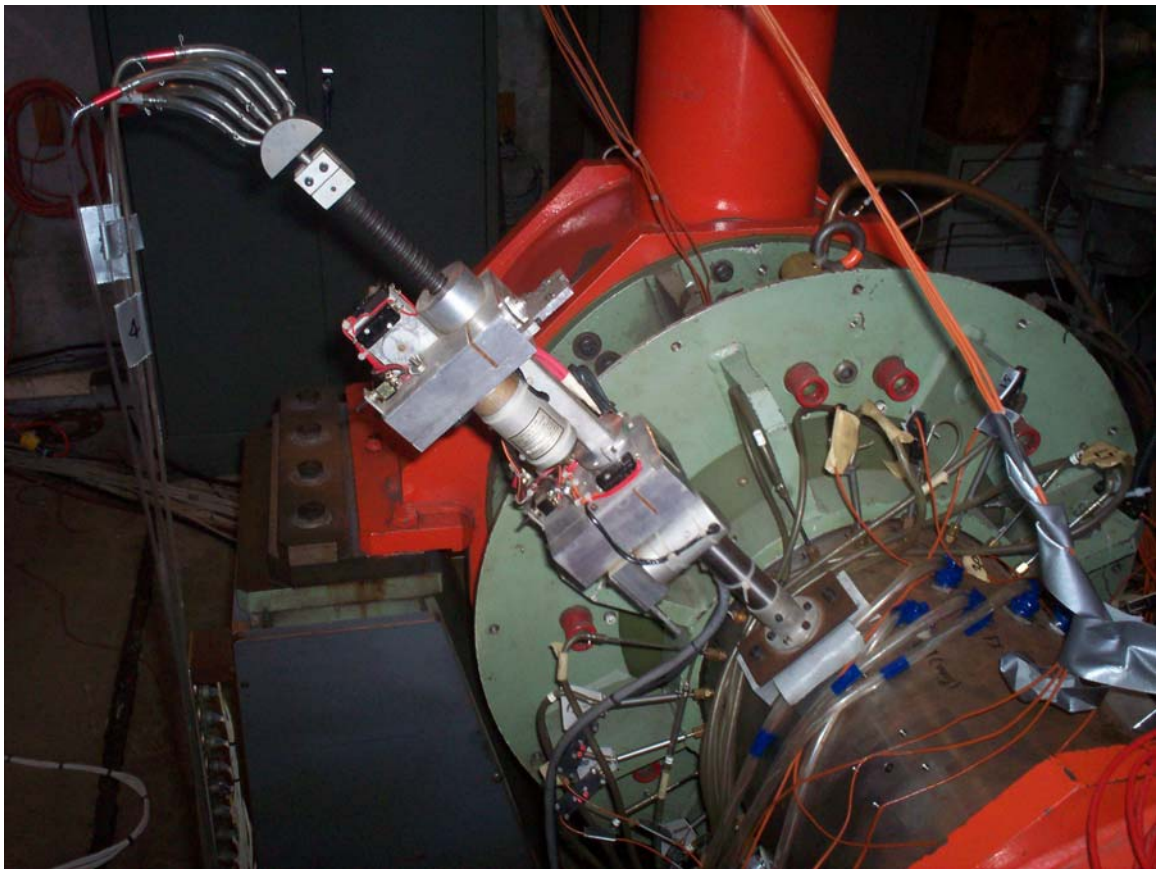

Figure 11. L.C. Smith probe actuator with five hole probe during testing

D. OMEGA PX-138 PRESSURE TRANSDUCERS

The Omega PX-138 Pressure transducers were used during experimentation. The transducers were temperature-compensated and used silicon pressure sensors which would measure gauge pressure changes as voltages. A pressure transducer is shown in Figure 12. The specific transducer used during experimentation was the PX138-015DV model capable of a differential pressure range of ±15 psi with a max error of ±.5 percent. (Omega, 2005)

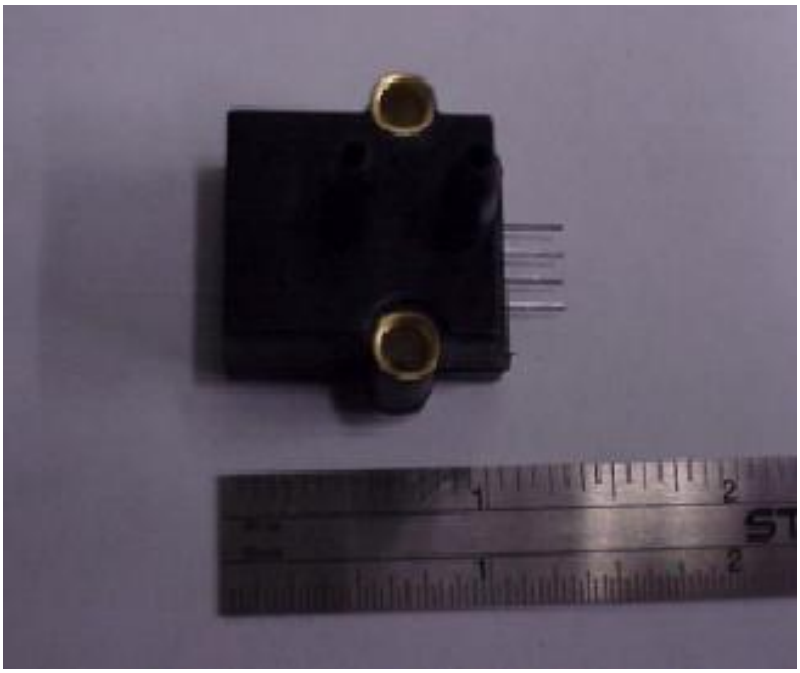

Figure 12. Omega PX-138 pressure transducer [From Ref. 2]

Seven pressure transducers were used for measurements in the TCR. Five transducers were dedicated for pressure measurements by the five-hole probe while the remaining two were used to measure inlet stagnation and static pressures. Each pressure transducer was independently calibrated. The transducers were connected to a regulated 8-Volt DC power supply. Improvements to the power supply box and transducer connections were made from previous setups by Villescas (2005) and Brunner (2005).

The seven transducers and two power supplies were mounted in a single box in the test cell. Excess wiring was removed and in order to minimize electrical loss and reduce resistance. A patch panel was installed to bring the pressure lines from the three and five-hole probes, and stagnation and static pressure lines to the transducers. This allowed for easy line connections and disconnections in order to move the box while calibrating the transducers. Contained in the new test box are the L.C. Smith actuator power supply, transducer power supply, patch panel for the seven incoming pressure lines, and the transducers themselves. The new test box is shown below Figure 13.

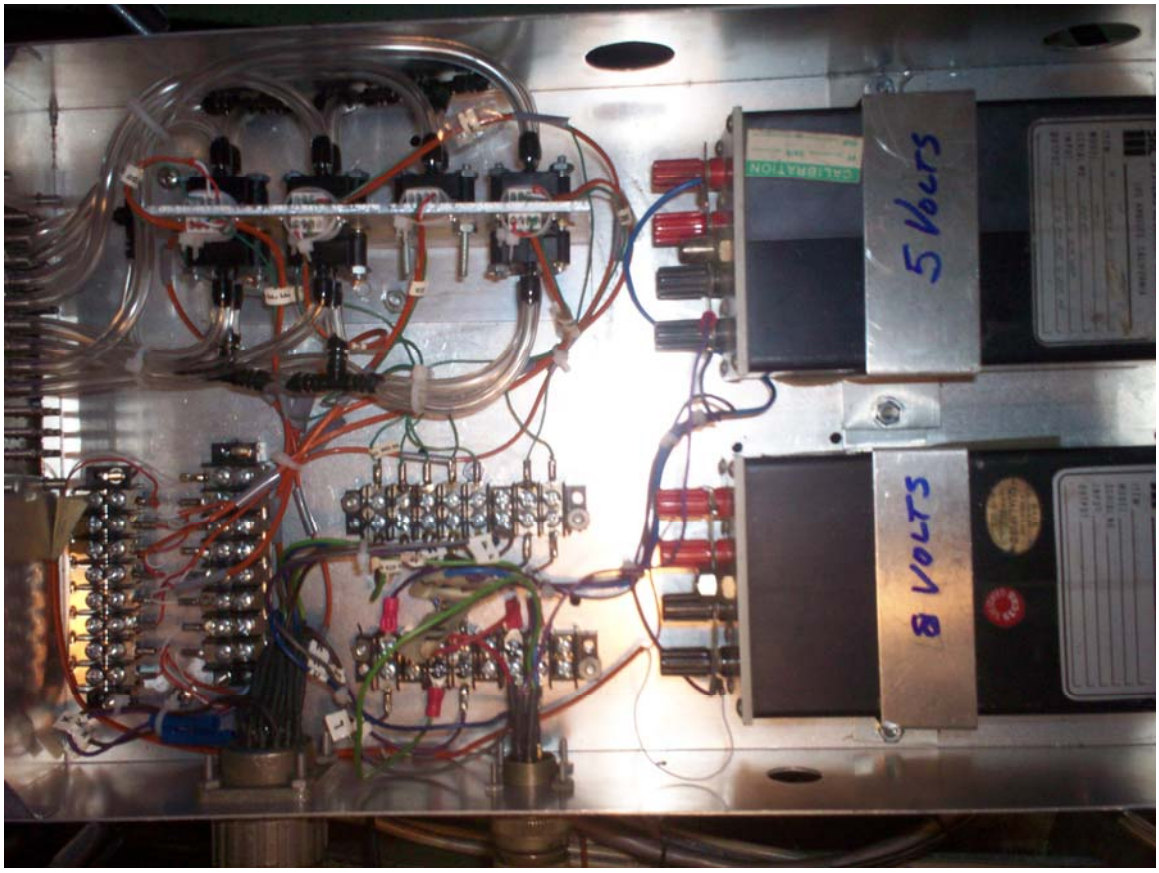

Figure 13. Pressure transducers and power supply

E. USB ERB-24 REMOTE RELAY CONTROLLER

The original USB ERB-24 Remote Relay Controller used by Villescas and Brunner was replaced with a duplicate of the original following a short of the control board. The new board is shown in Figure 14. The USB ERB-24 Remote Relay Controller Board was used to connect the L.C. Smith actuator to a PC via a USB 2.0 port. The USB ERB-24 was an electromechanical relay with 24 single pole, double throw relays. It was configured in two banks of eight relays and two banks of four relays. Each relay had a minimum closed time of ten milliseconds and a minimum open time of five milliseconds. (Measurement Computing "USB ERB-24", 2005) The controller was called and activated using a MATLAB driver written by Villescas (2005).

Figure 14. USB ERB-24 controller

F. PMD-1608FS DATA ACQUISITION DEVICE

The Personal Measurement Device™ (PMD) 1608FS Data Acquisition Device is an eight channel USB analog to digital converter which translated the pressure transducer and probe actuator signals into digital data in a PC via a USB interface. (Measurement Computing "PMD-1608FS", 2005)

Two PMD-1608 modules were called and controlled via a MATLAB control command, separate from the USB-ERB 24. One module was responsible for data from the two motors on the probe actuator as well as the five pressure transducers corresponding to the pressure ports on the five-hole probe. The second module relayed data from the inlet stagnation and static pressure probes. The wiring schematic for both the USB ERB-24 and PMD-1608FS is shown in Figure 15.

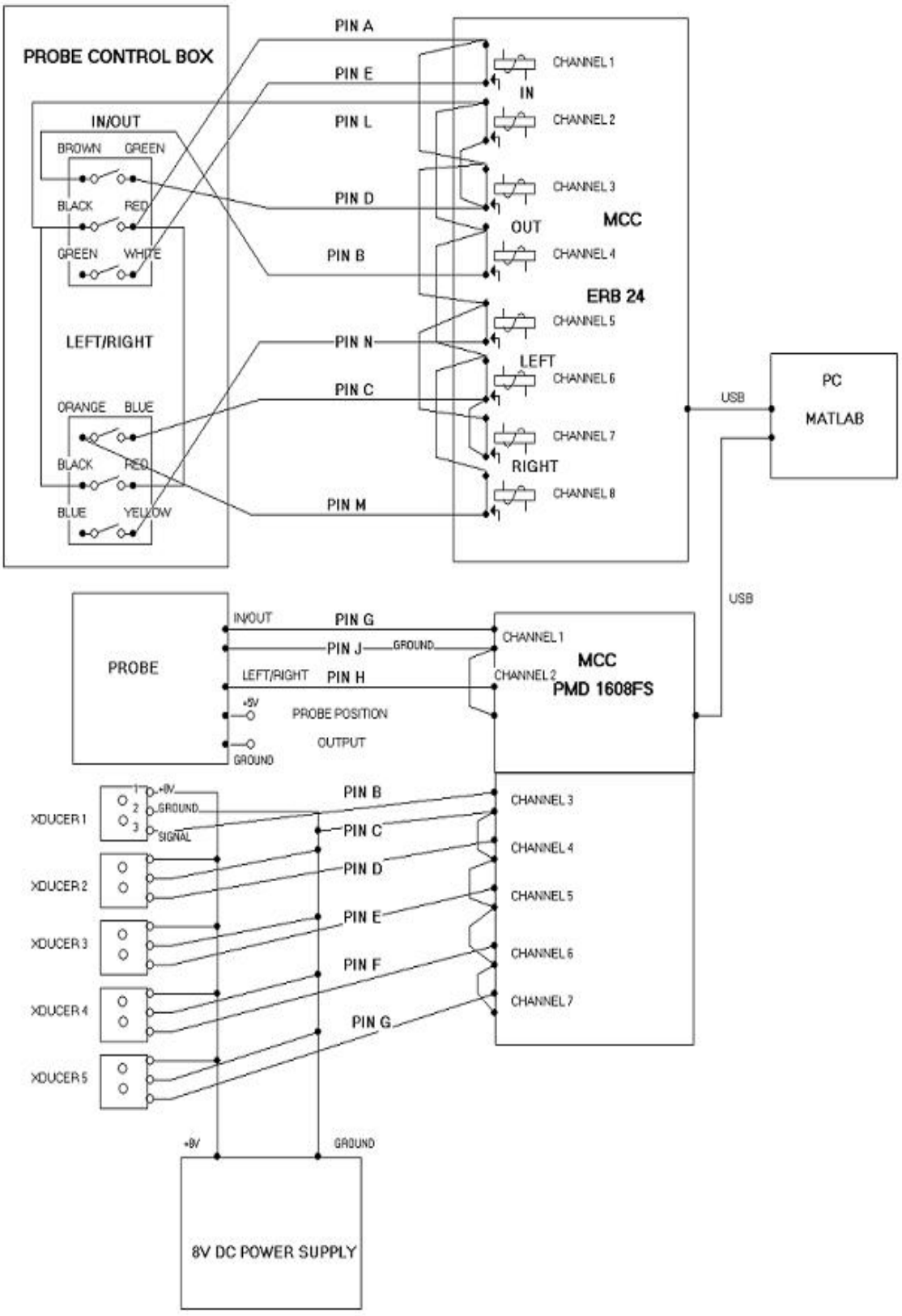

Figure 15. Wiring schematic for pressure acquisition and actuator control [From Ref. 2]

G. MATLAB

MATLAB version 6.5, Release 13 was used to run all programs used in calibration and experimental measurements of the five-hole probe. The data acquisition programs and graphical user interface were created by Villescas (2005) and modified by Brunner (2005) to allow for the two additional pressure transducers. The programming is explained in detail by Villescas and modifications to accommodate the extra transducers by Brunner. These programs controlled actuator movements, took readings from the seven pressure transducers and exported the data into an Excel spreadsheet for post-processing.

IV. TEST RUN PROCEDURE

A. OVERVIEW

The L.C. Smith probe actuator was used to control both three and five-hole probes in the upstream and downstream flow surveys. The actuator was mounted to the Transonic Compressor case wall and inserted to various depths, taking measurements at varying speeds and mass flow rates.

Data were taken to compare to data taken by Villescas and Brunner in order to determine the effects of the new honeycomb filter placed at the inlet of the Transonic Compressor. The data was used to determine if the previously established operational parameters were still valid or whether they would become the new baseline data for which future experiments could calculate the effects of steam ingestion on stall margin and rotor performance.

B. PROCEDURE

The procedure for the three- and five-hole probe survey was the same as that described in Villescas and Brunner. Upon inserting the probe into the flow, the probe was balanced by equalizing the pressures on pressure ports two and three on the five-hole probe and one and three on the three-hole probe. A survey was performed on the flow field covering thirteen locations in the field. Due to the width of the five-hole probe it could not be inserted as far into the flow-field given the configuration of the downstream mountings on the case wall. Thirteen locations were still used downstream of the rotor during the survey, but the locations were located in closer proximity to each other. A table of sampling positions is shown in Table 2. (Brunner, 2005)

Position Number	Upstream Survey Radial Depth (cm)	Downstream Survey Radial Depth (cm)
1	10.86	2.14
2	9.36	2
3	7.91	1.75
4	6.54	1.51
5	5.26	1.27
6	4.09	1.06
7	3.05	0.85
8	2.14	0.67
9	1.38	0.49
10	0.78	0.36
11	0.35	0.22
12	0.09	0.14
13	0	0

Table 2. Five-hole probe sampling positions

The three-hole probe was implemented as described by Villescas upstream of the compressor in efforts to determine the effect of the new honeycomb at the inlet of the Transonic Compressor. The sampling locations are shown in Table 3.

Position Number	Upstream Survey Radial Depth (cm)
1	13.97
2	12.41
3	10.86
4	9.36
5	7.91
6	6.54
7	5.26
8	4.09
9	3.05
10	2.14
11	1.38
12	0.78
13	0.35
14	0.09
15	0

Table 3. Three-hole probe sampling locations

V. EXPERIMENTAL RESULTS

A. PERFORMANCE MAP

The changes to the inlet of the rig changed the operating parameters of the compressor. A new performance map was plotted against the original operating parameter and is shown below in Figure 16. The new stall lines as well as operating curves are labeled against the previous data. At 90 percent speed and open throttle the mass flow rate had increased by two percent. This was most probably due to the cleaning of blocked pressure lines to the inlet flow rate nozzle. At peak pressure rise close to stall the characteristic seemed unchanged. However, the stall line was displaced to the right by four percent.

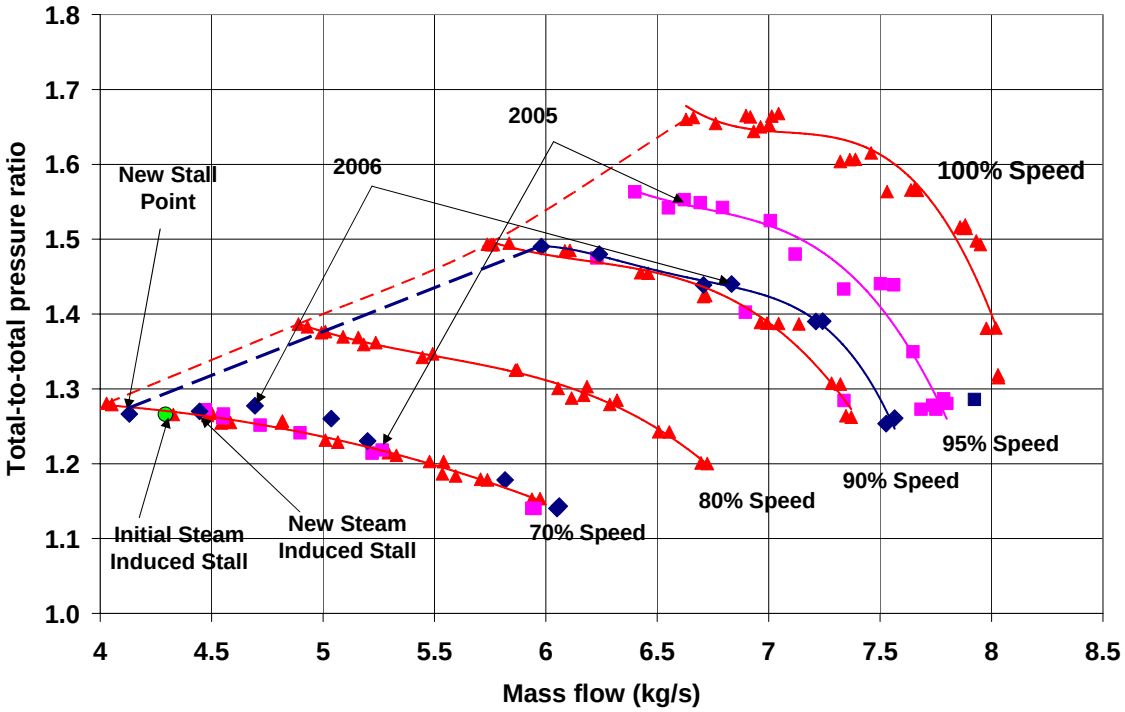

Figure 16. Compressor performance map

B. REPEAT STEAM INGESTION RUN

A repeat of the 70 percent steam ingestion run was performed, which can be seen in Figure 16 as the new steam induced stall point. The plot of temperature and pressure as

a function of time during the steam dump can be seen in Figure 17. From the change in pressure with time, mass flow rate of the steam through the compressor was determined to be .045 kg/sec.

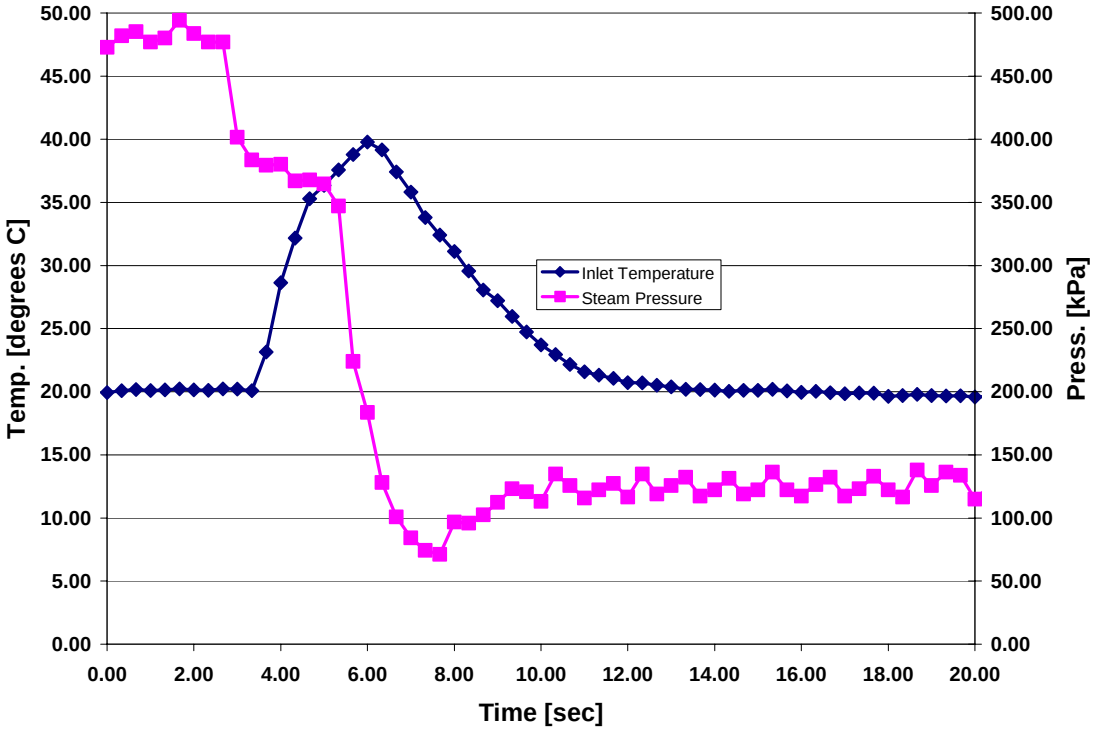

Figure 17. Transient temperature and pressure response during a steam ingestion run

C. THREE HOLE DATA

Upstream flow field data obtained from the three-hole probe was plotted against previous results from Villescas (2005). The plots of Mach number at varying probe depth are shown in figures 18 to 23, for 70 and 90 percent speeds, at varying mass flow rates.

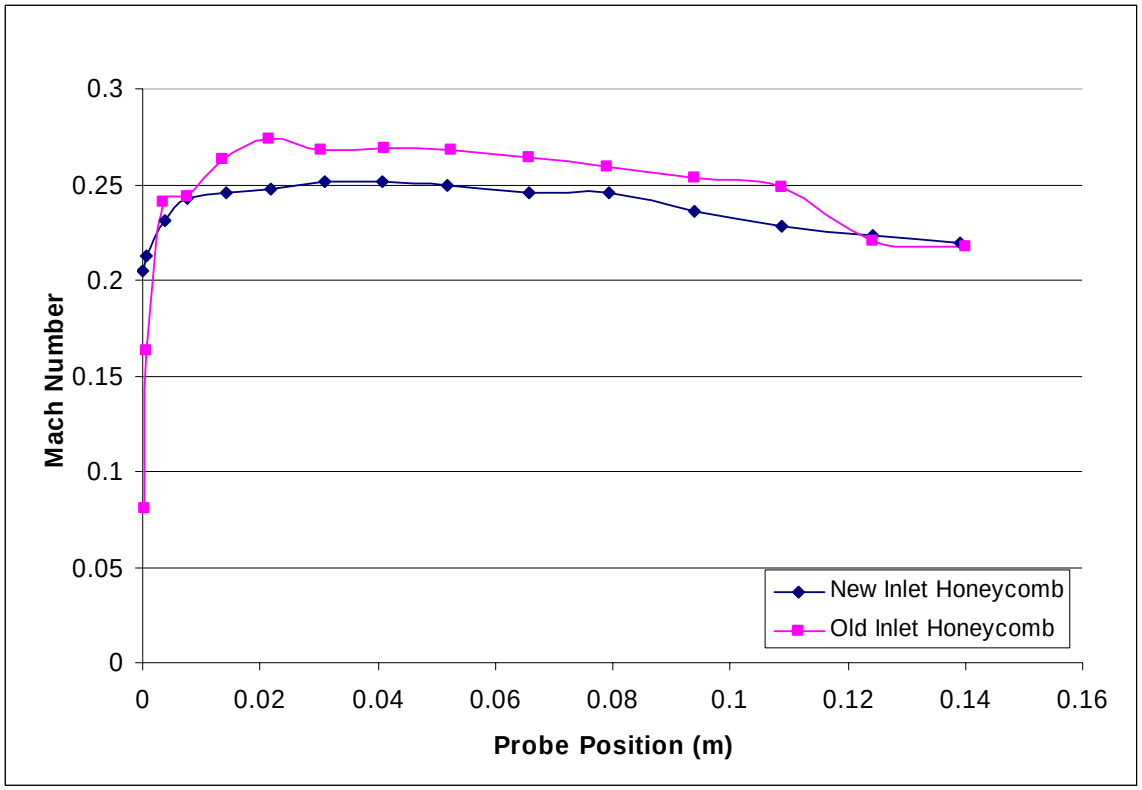

Figure 18. Mach number distribution at 70%, speed open throttle condition

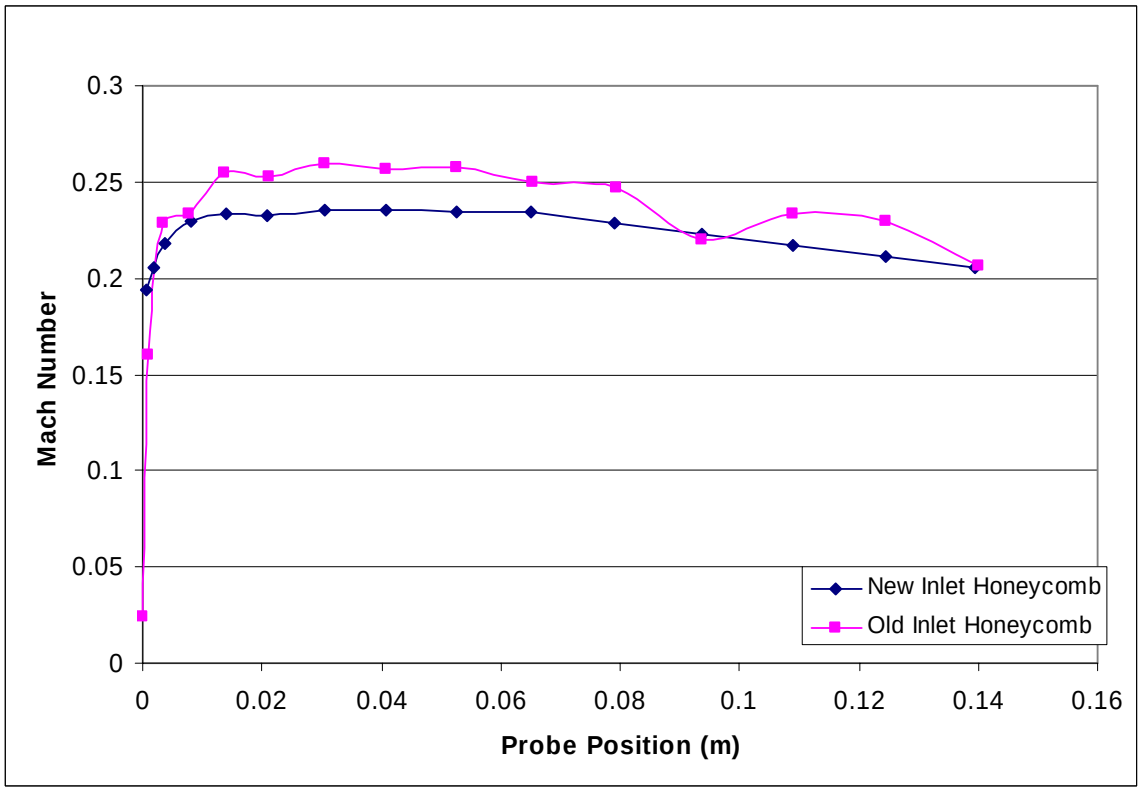

Figure 19. Mach number distribution at 70% speed peak efficiency condition

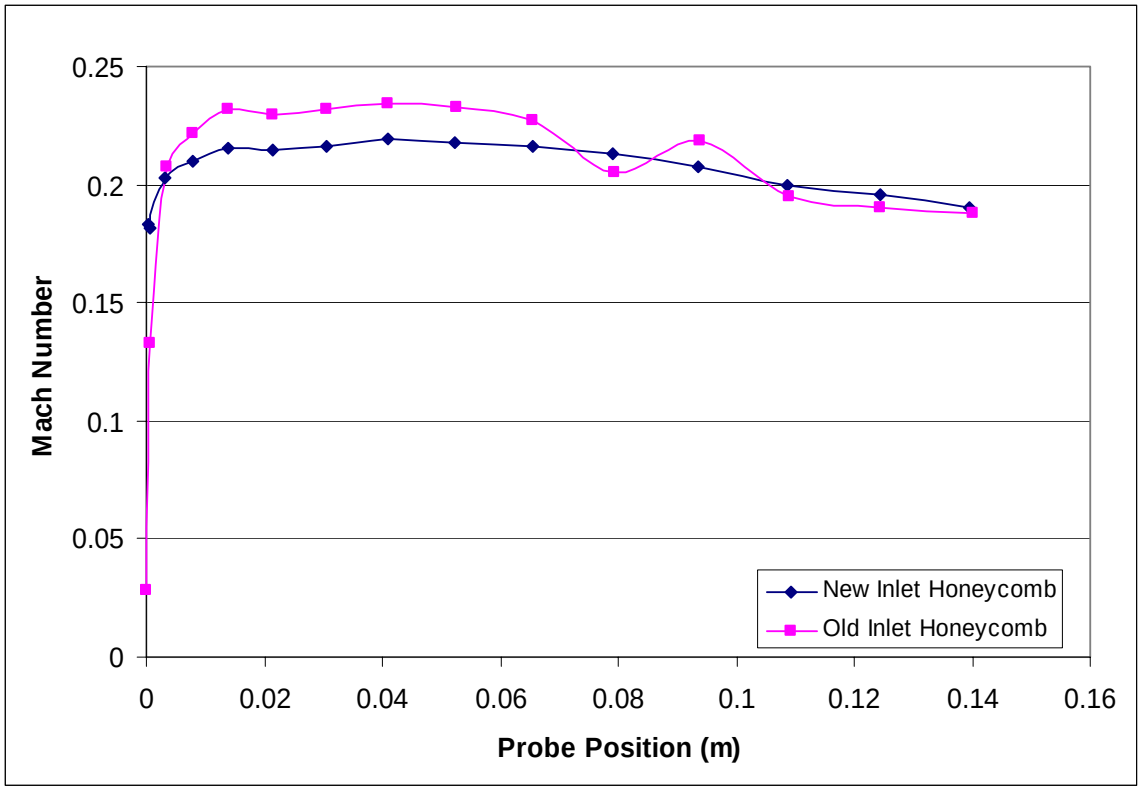

Figure 20. Mach number distribution at 70% speed, near stall condition

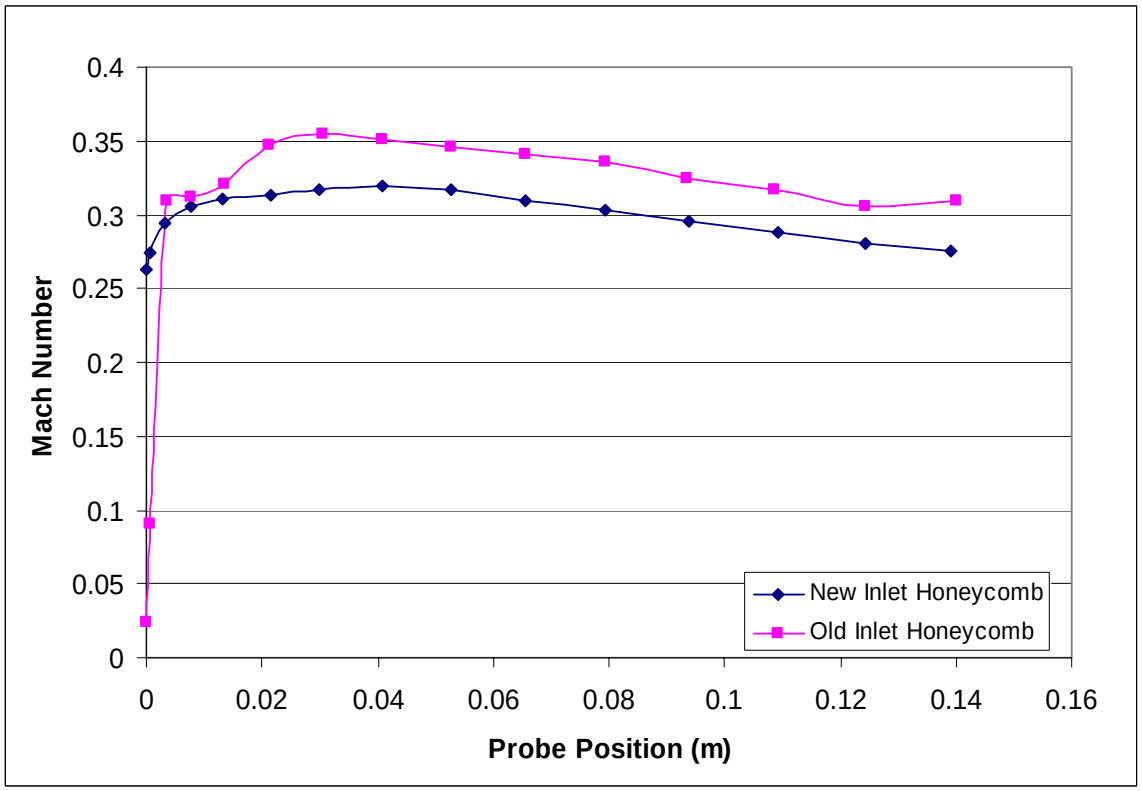

Figure 21. Mach number distribution at 90% speed, open throttle condition

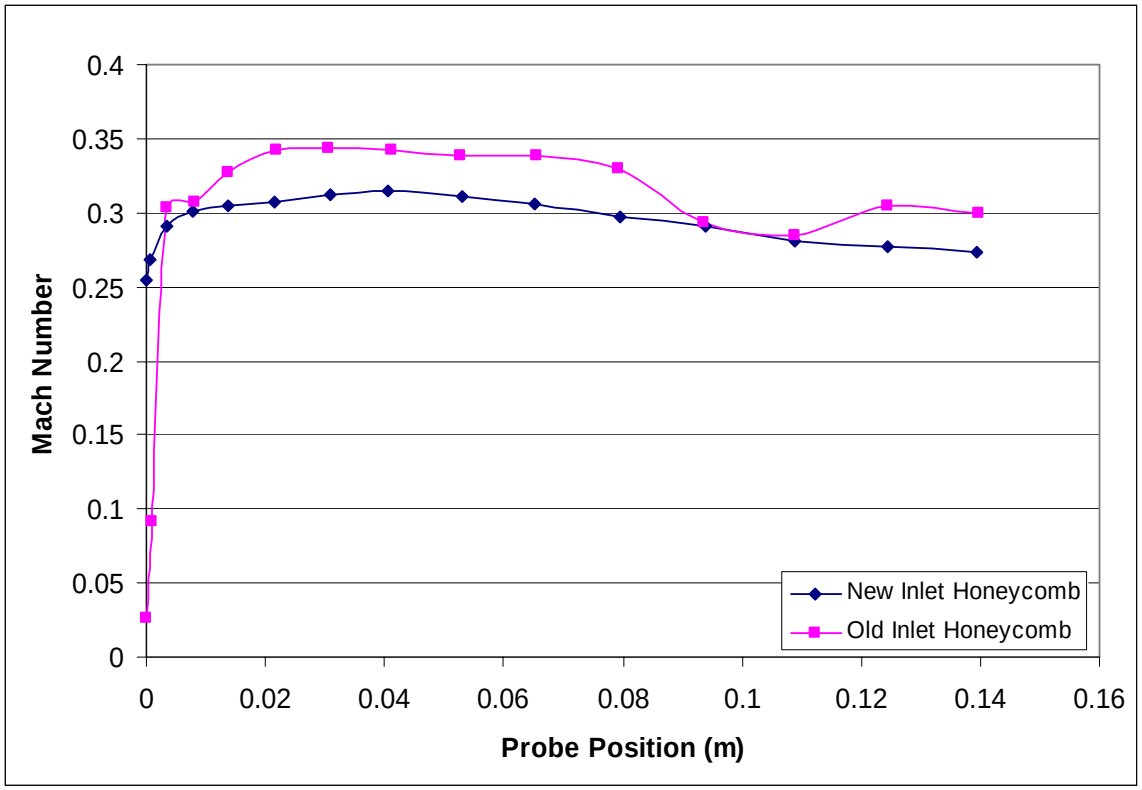

Figure 22. Mach number distribution at 90% speed, peak efficiency condition

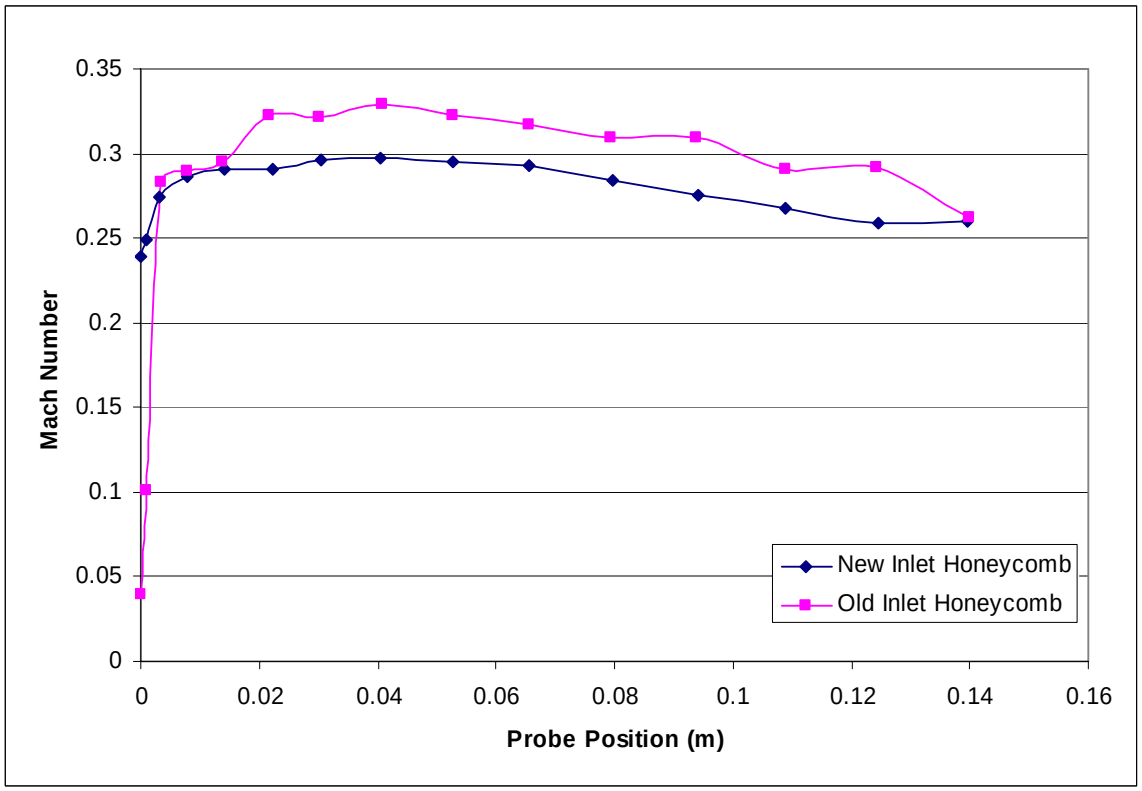

Figure 23. Mach number distribution at 90% speed, near stall condition

Three-hole data was then integrated to back out a mass flow rate based on static pressure and Mach number at 70 and 90 percent open throttle conditions. The corrected mass flow rate for the current data was found to be 5.99 kg/sec at 70 percent speed and 7.51 kg/sec at 90 percent design speed. These values confirm the current location on the compressor map shown in Figure 16. The same calculations were performed on data from Villescas (2005) and resulted in corrected mass flow rates of 6.31 and 8.40 kg/sec for the 70 and 90 percent design speeds, respectively. These points are well to the right of the open throttle conditions on the compressor map.

Data obtained from the three-hole probe was also used to calculate the pressure drop across the inlet of the transonic compressor. The pressure drop was then compared to the inlet pressure drop as existed with the previous inlet honeycomb. (Villescas, 2005) The plots of the pressure drop versus probe position are shown below for 70 and 90 percent design speeds at varying mass flow rates are shown in Figures 24 and 25.

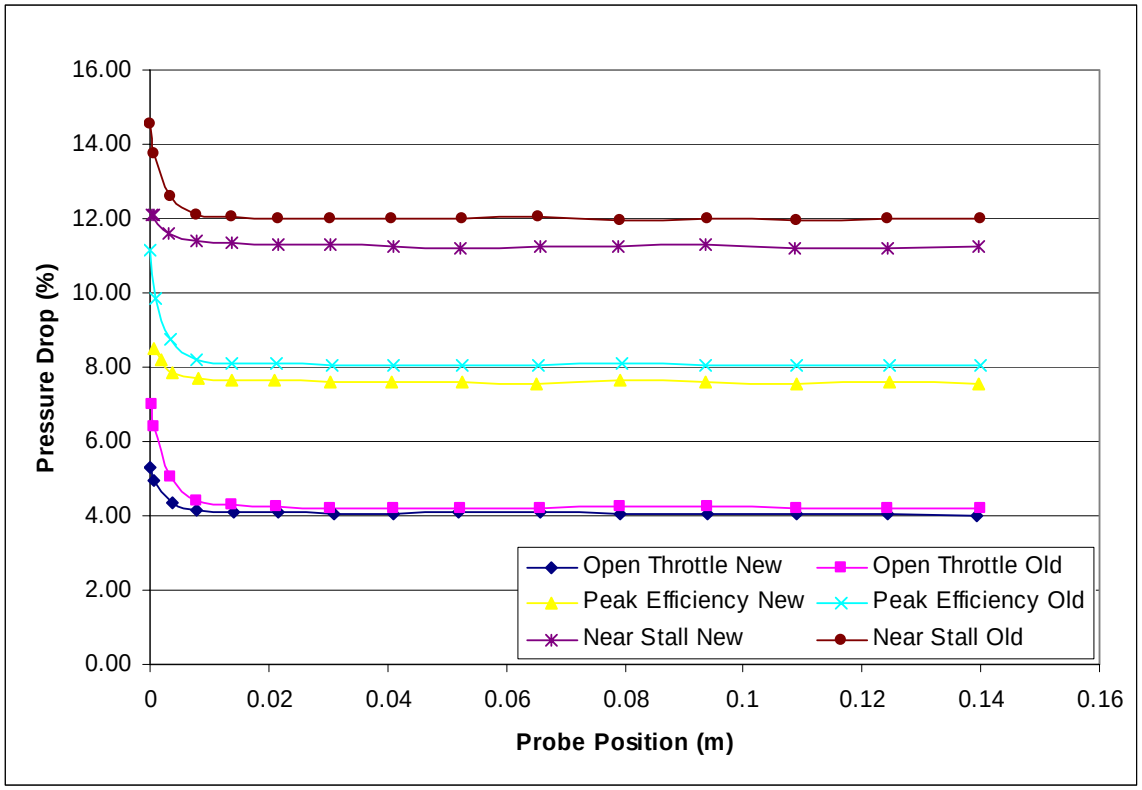

Figure 24. Pressure drop across the compressor inlet at 70% speed

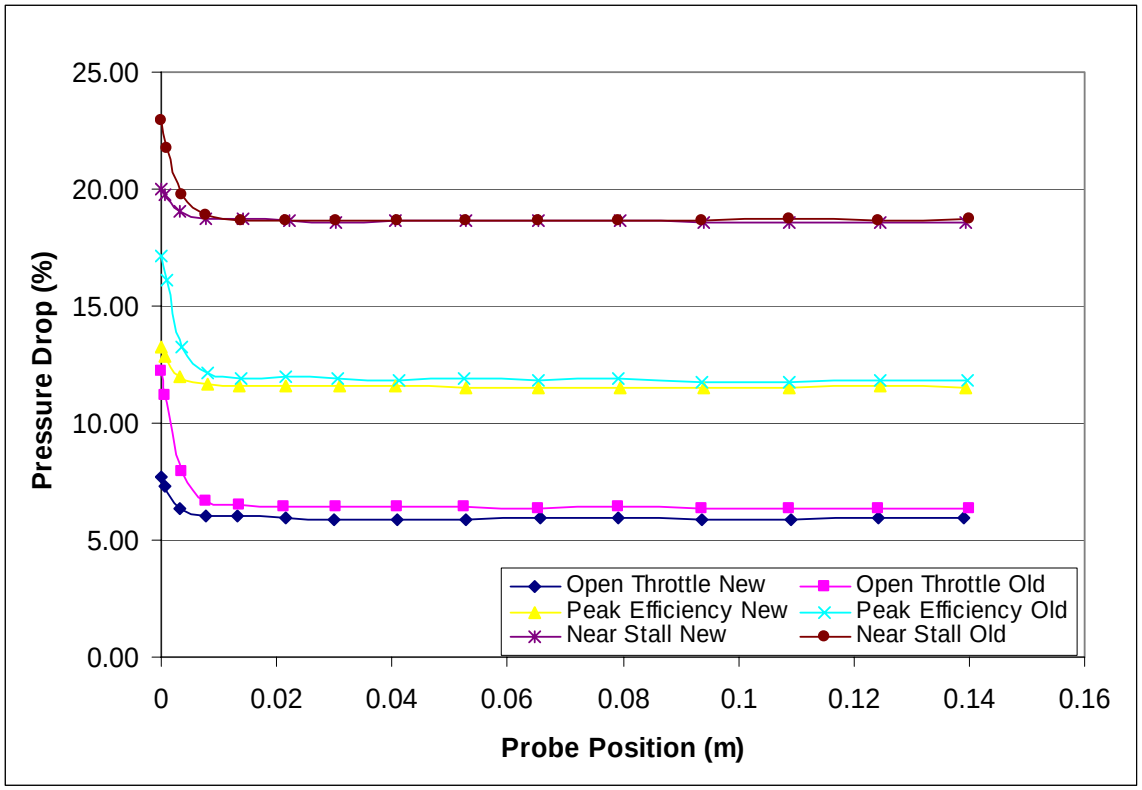

Figure 25. Pressure drop across the compressor inlet at 90% speed

The largest difference between the present and Villescas data occurred at 70 percent speed near stall where the old inlet honeycomb accounted for a 10 percent greater pressure drop. At 90 percent there was no discernable difference in pressure drop over the inlet honeycombs.

D. FIVE-HOLE DATA

The five-hole probe was used to collect data upstream and downstream of the Sanger rotor. Upstream Mach numbers were computed from the measured pressures and plotted versus data from Brunner (2005) for 70 and 90 percent design speeds at open throttle, peak efficiency and near stall conditions. The plots are shown in Figures 26 thru 31.

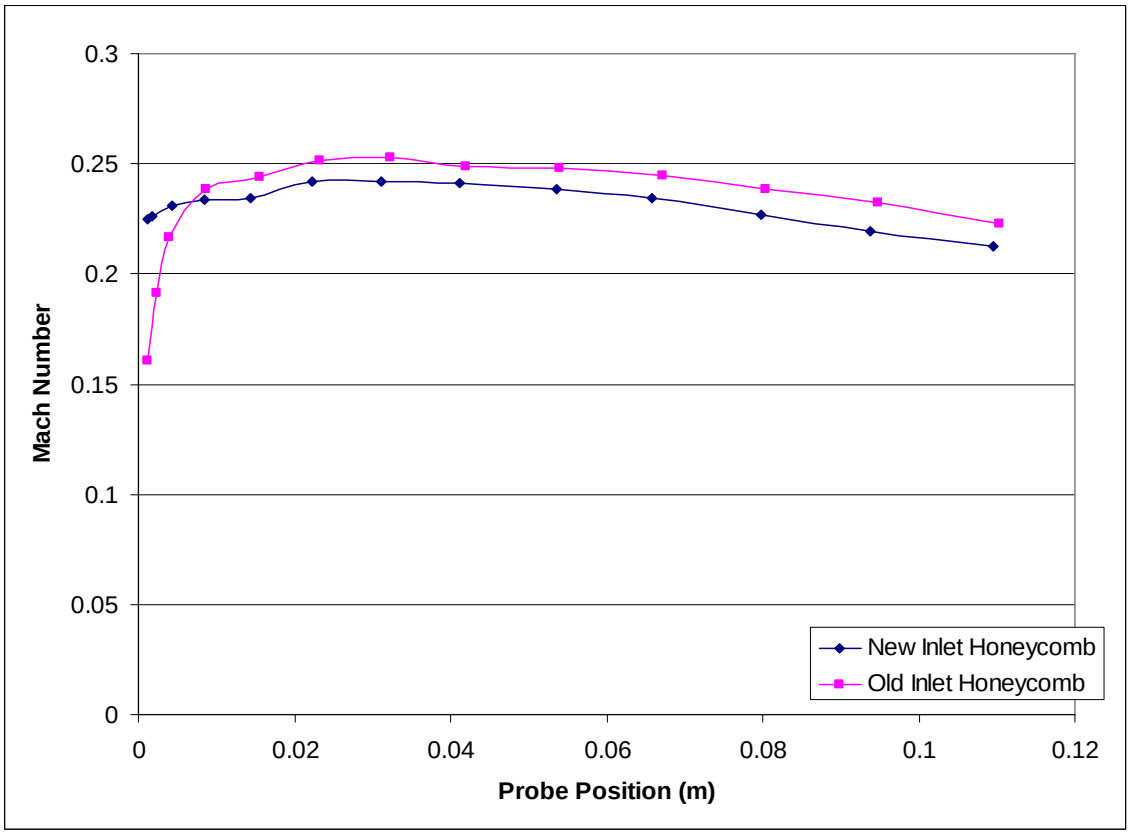

Figure 26. Mach number distribution at 70% speed, open throttle condition

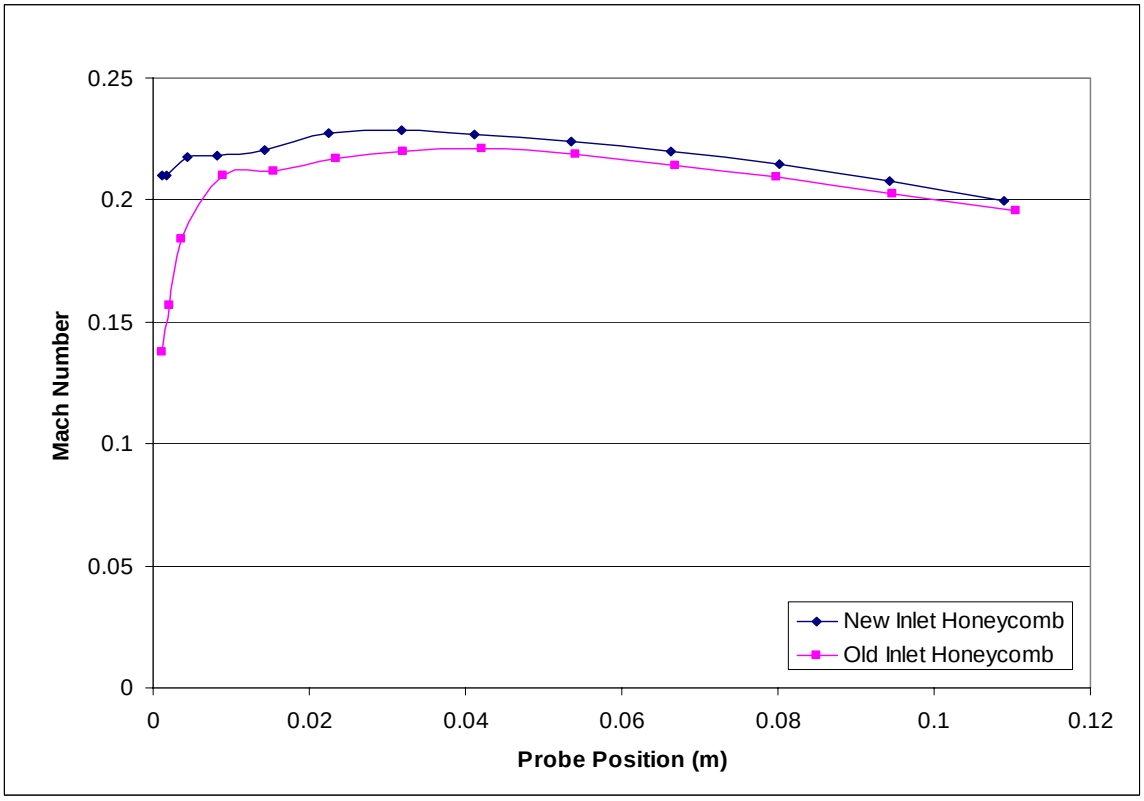

Figure 27. Mach number distribution at 70% speed, peak efficiency condition

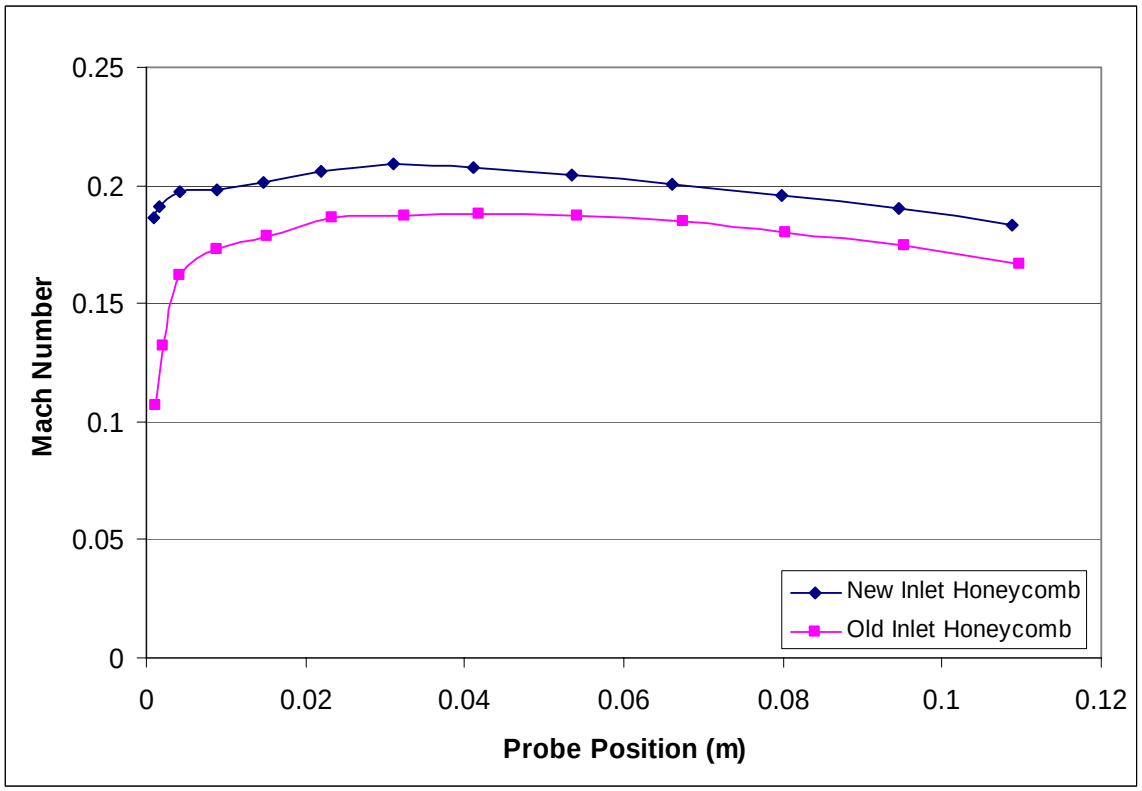

Figure 28. Mach number distribution at 70% speed, near stall condition

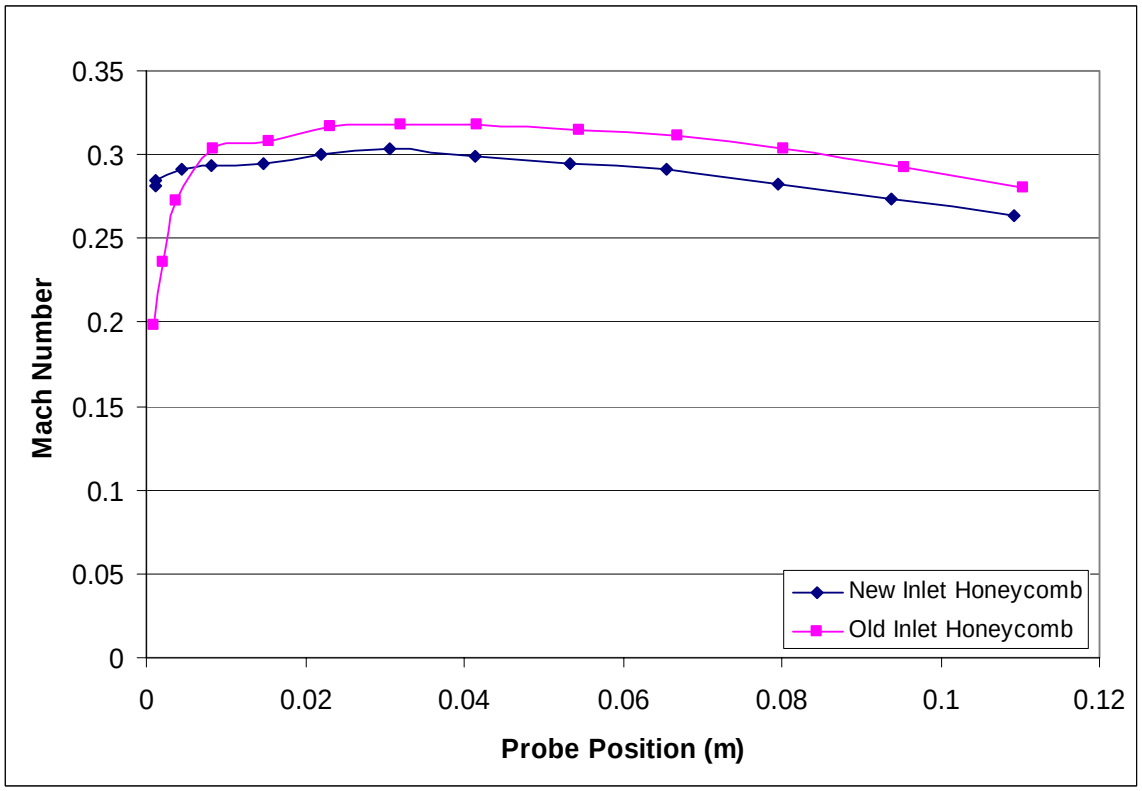

Figure 29. Mach number distribution at 90% speed, open throttle condition

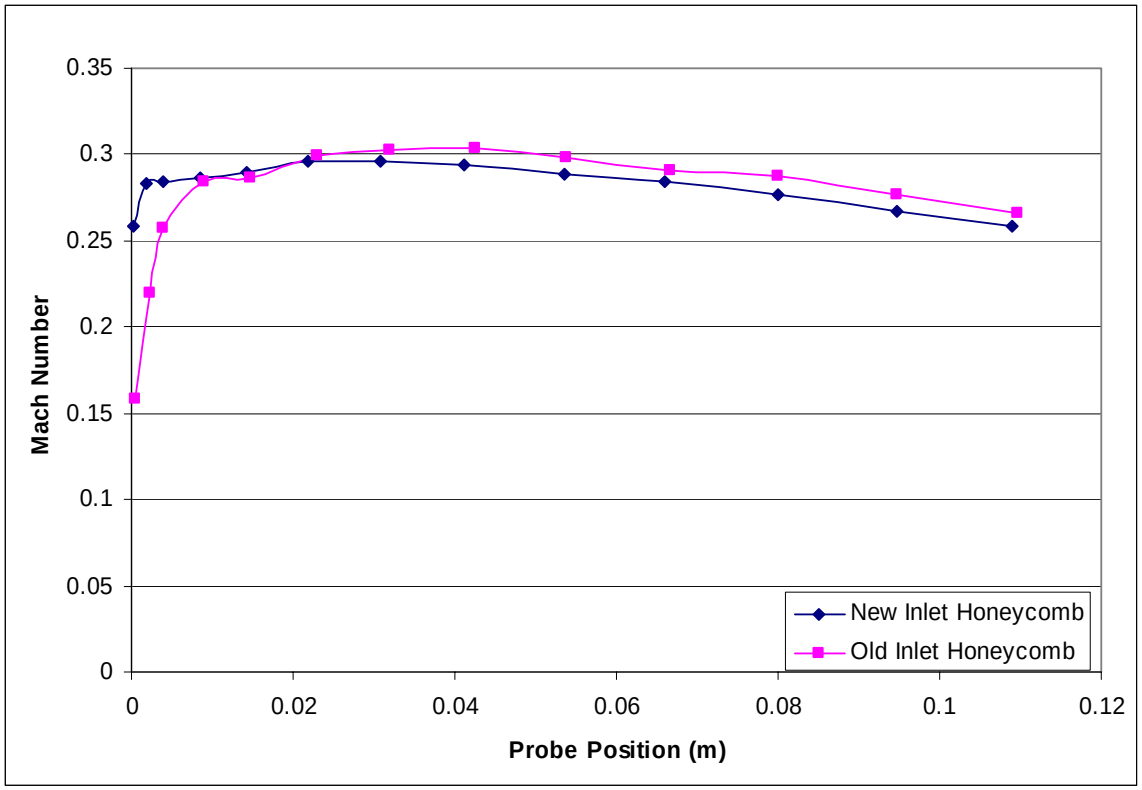

Figure 30. Mach number distribution at 90% speed, peak efficiency condition

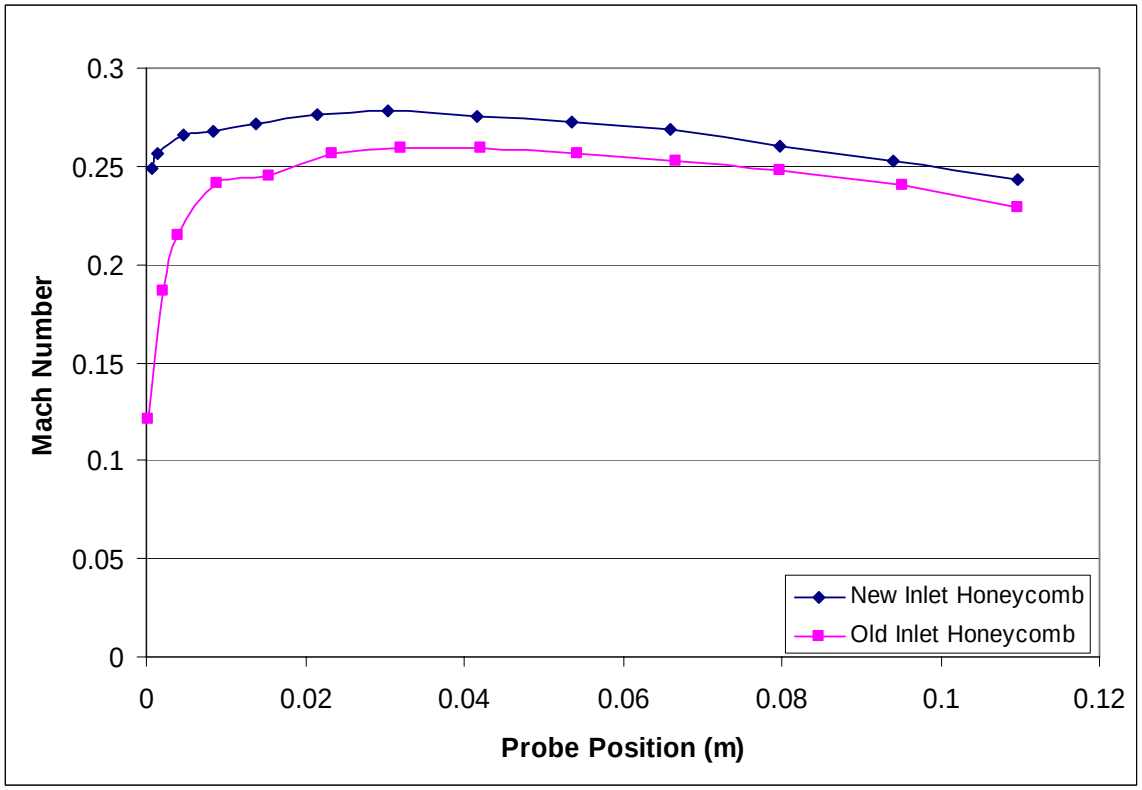

Figure 31. Mach number distribution at 90% speed, near stall condition

The five-hole probe was also used to perform a flow-field survey downstream of the rotor. Mach numbers were computed at 70 percent design speed for varying flow conditions and are show in Figures 32 thru 34.

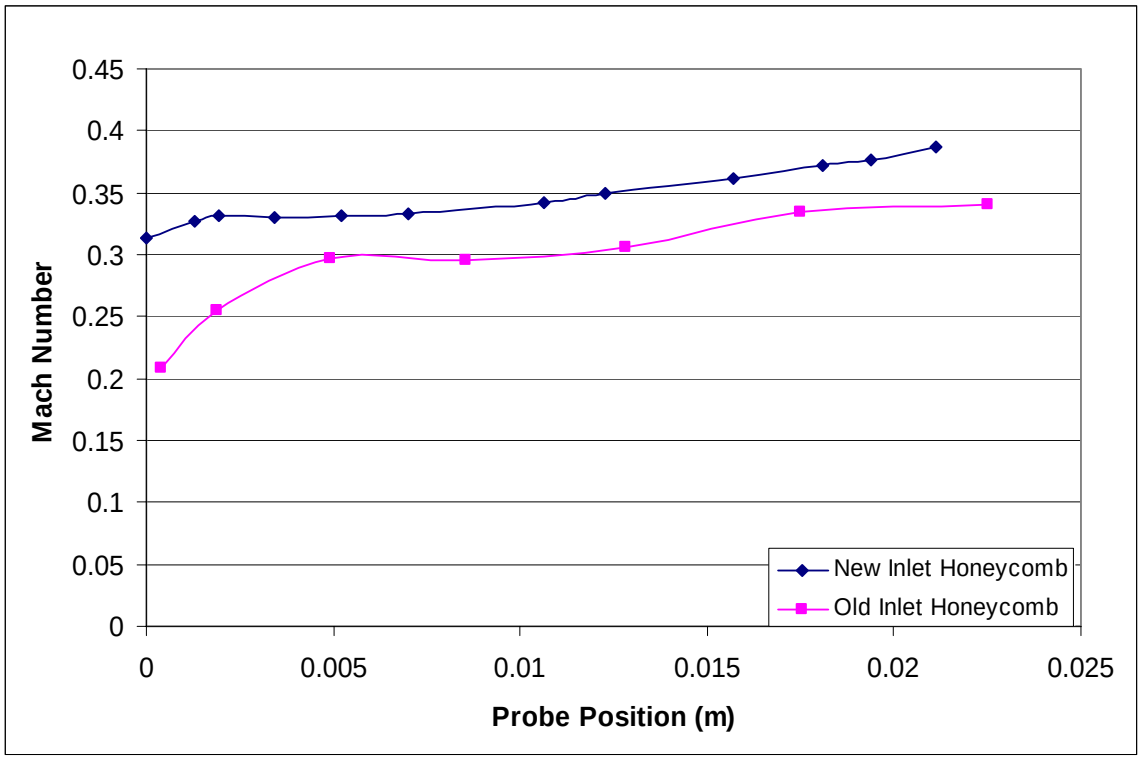

Figure 32. Downstream Mach number distribution at 70% speed, open throttle condition

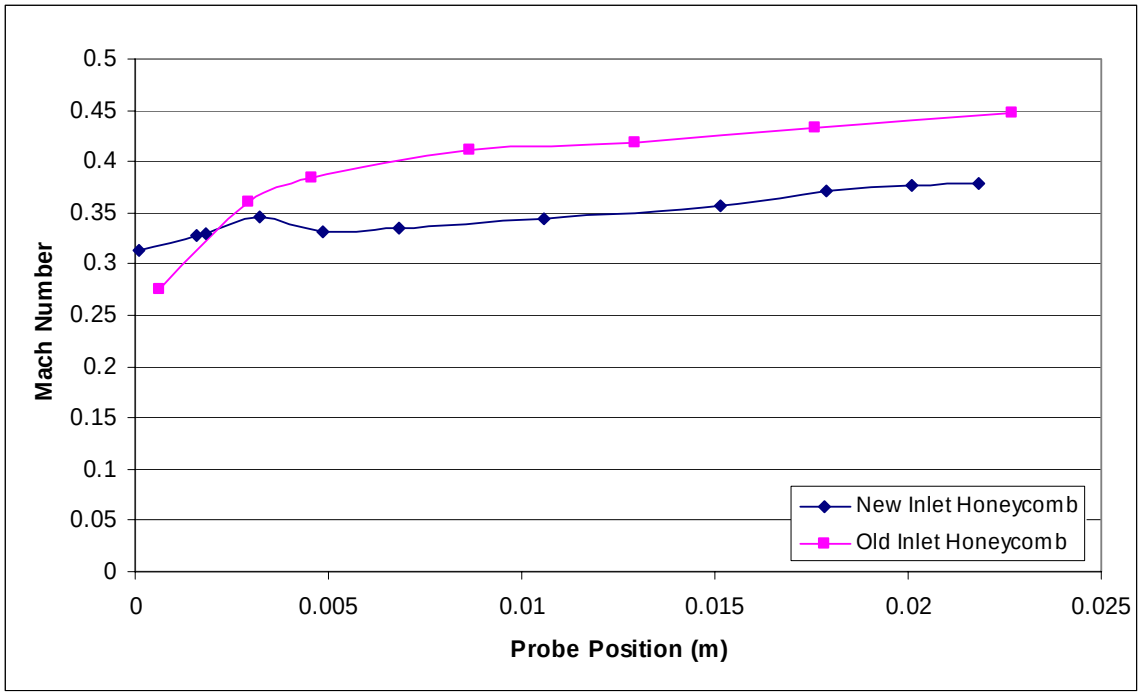

Figure 33. Downstream Mach number distribution at 70% speed, peak efficiency condition

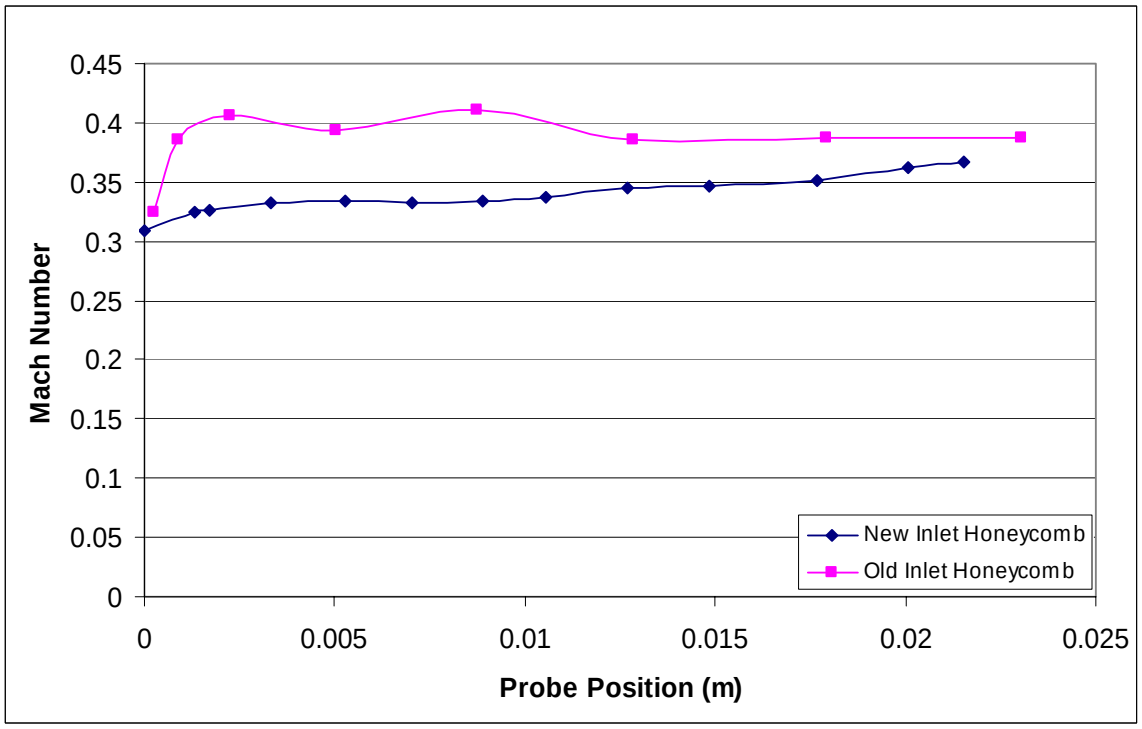

Figure 34. Downstream Mach number distribution at 70% speed, near stall condition

The flow angles downstream of the rotor were plotted against downstream data from Villescas (2005) and are shown in Figures 37 thru 39.

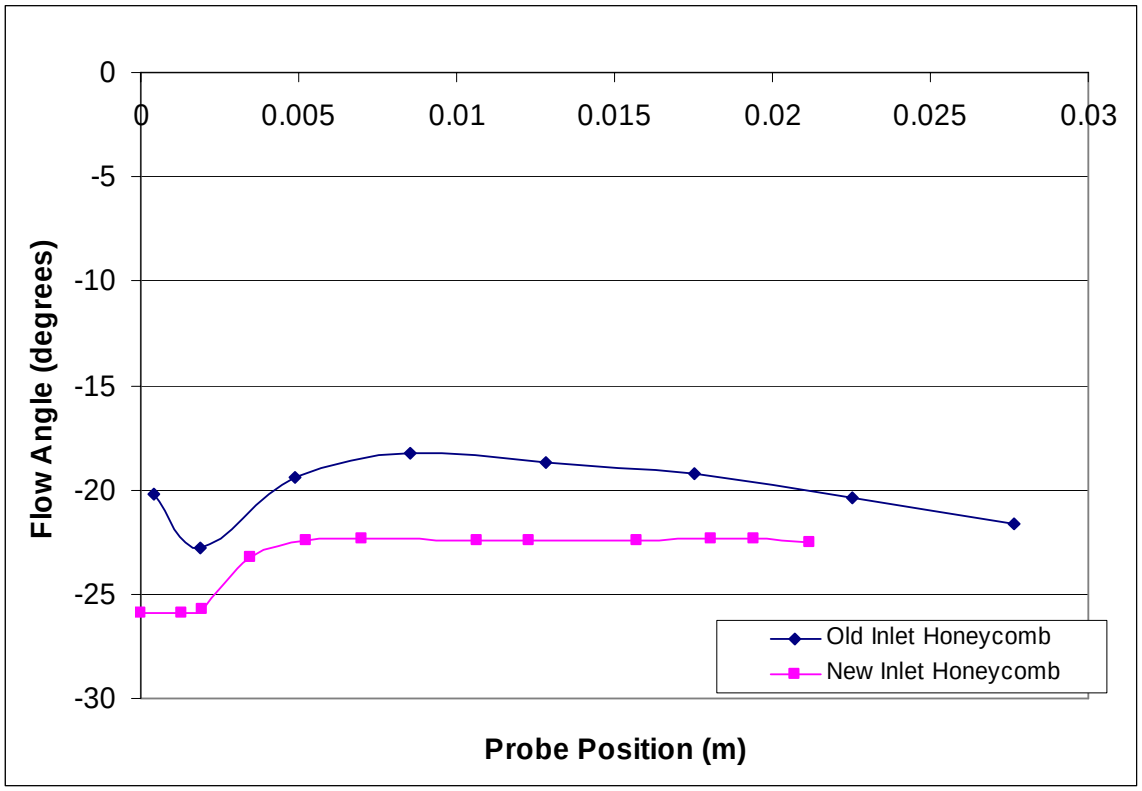

Figure 35. 70 % speed open throttle downstream flow angle

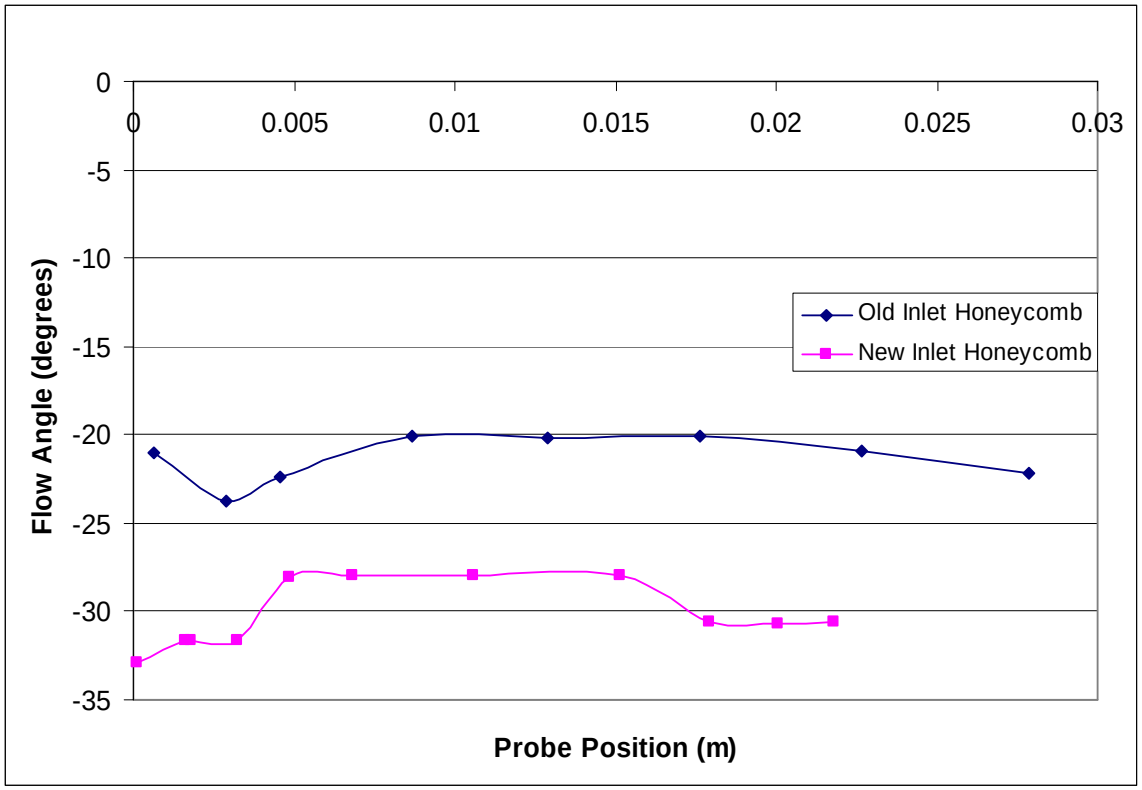

Figure 36. 70 % speed peak efficiency downstream flow angle

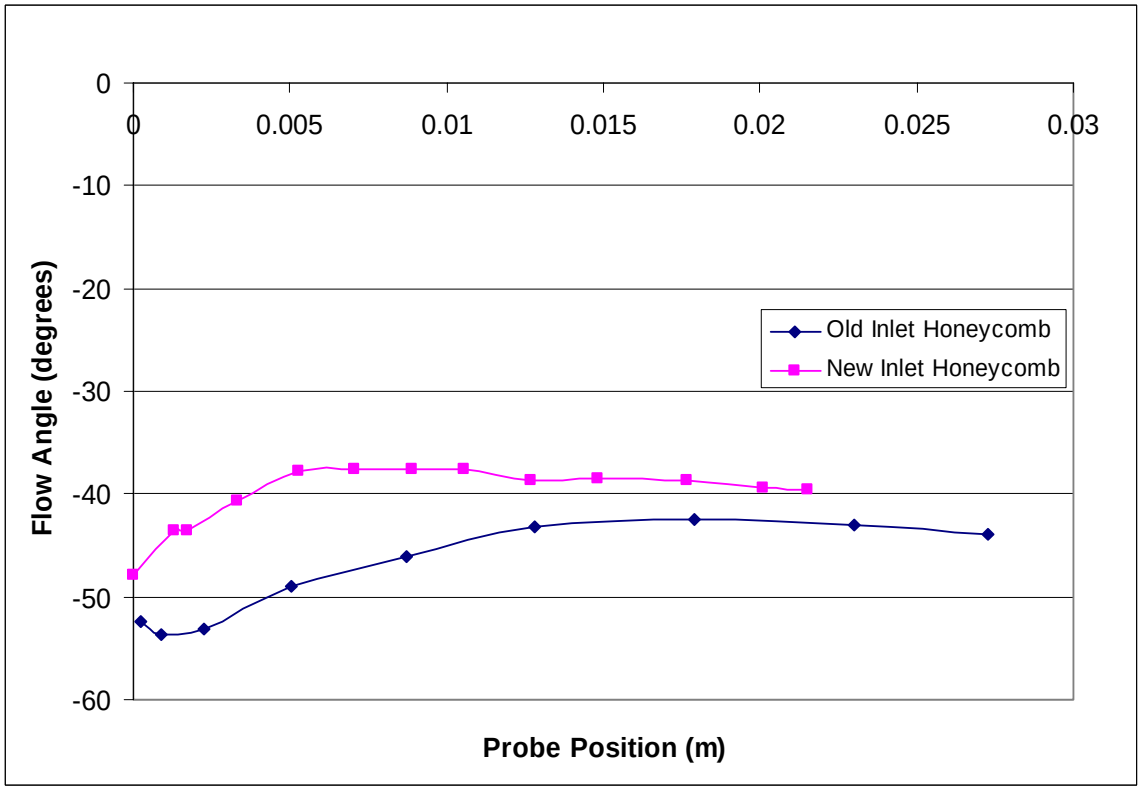

Figure 37. 70 % speed near stall downstream flow angle

VI. CONCLUSIONS

The changes to the inlet of the transonic compressor rig have changed the characteristics of the flow. Tracing the new compressor performance map was an essential function before moving on with steam ingestion studies, by designating the new operating parameters and establishing the new stall line. The mass flow rate characteristics have increased at choke for both the 70 and 90 percent speed curves. The stall line has also shifted to the right, due to changes to the new honeycomb upstream of the compressor as well as the cleaning out of all pressure lines.

The three-hole probe was the same probe used by Villescas during prior experimentation. The Mach numbers have decreased a noticeable amount indicating that the flow field has definitely changed. The three-hole probe determined inlet-flow profile and was integrated to calculate a mass flow rate through the compressor at 70 and 90 percent open throttle condition. The corrected mass flow rate compared very well with that measured by the inlet flow rate nozzle. The five-hole probe was a different probe than that used by Brunner but the results still showed a change in the flow through the TCR. Measurements taken with the five-hole probe showed a similar trend in the flow angle downstream of the rotor to those previously seen.

The difference in measurements between the three and five-hole probes can likely be accounted for by the shape of the probes themselves. The three-hole probe openings point away from the shaft of the probe into the flow, reducing effects of the large shaft on readings. The five-hole probe openings are located on the same axis as the shaft and disturbances to the flow arise as the flow passes the probe.

THIS PAGE INTENTIONALLY LEFT BLANK

VII. RECOMMENDATIONS

In future studies, the five-hole probe should be used to perform a full survey downstream of the rotor. To accomplish this, the probe access holes in the case wall must be widened to accommodate the shaft of the probe so it has the ability to traverse the entire flow. The five-hole probe is necessary to determine flow pitch both downstream of the rotor due to rotor assembly and at the inlet when steam is introduced. It is also recommended to replace the Scanivalves and Omega PX-138 Transducers with a Digital Sensor Array for real-time pressure data.

THIS PAGE INTENTIONALLY LEFT BLANK

LIST OF REFERENCES

1. Anderson, D.J., Olsen, J.A., Shreeve, R.P., 1977, “Velocity Vector Determination from Multiple-Sensor Pneumatic Probe Measurements,” AIAA 1977, 9th Fluid and Plasma Dynamics Conference, San Diego California

2. Brunner, M.D., Comparison of experimental and Computational Measurements of Flow in a Transonic Compressor Inlet, Master's Thesis, Naval Postgraduate School, Monterey, California, September 2005.

3. Donelson, S. Briggs, T., "*JSF Team Probes Steam Catapult Environment*," JSF Integrated Test Force, dcmilitary.com, February 6, 2003.

4. Gannon, A.J., Hobson, G.V., Shreeve, R.P., “Measurement of the Unsteady Casewall Pressures Over the Rotor of a Transonic Fan and Comparison with Numerical Predictions", ISABE 2005, 17th International Symposium on Airbreathing Engines, Munich, September 2005.

5. Measurement Computing, PMD-1608FS USB Based Analog and Digital I/O Module User's Guide. May 6, 2005.

6. Measurement Computing, USB-ERB24 USB Based 24 Relay Module User's Guide. May 4, 2005.

7. O’Brien, J.M., Transonic Compressor Test Rig Rebuild and Initial Results with the Sanger Stage, Master's Thesis, Naval Postgraduate School, Monterey, California, June 2000.

8 Payne, T., Inlet Flow-Field Measurements of a Transonic Compressor Rotor Prior to and During Steam-Induced Rotating Stall, Master’s Thesis, Naval Postgraduate School, Monterey, California, December 2005.

9. Papamarkos, I., Inlet Distortion Generation for a Transonic Compressor , Master’s Thesis, Naval Postgraduate School, Monterey, California, September 2004.

10. Sanger, N. L., "Design of a Low Aspect Ratio Transonic Compressor Stage Using CFD Techniques," ASME Journal of Turbomachinery, July 1996, Vol. 118 pp 479-491.

11. Sussman Automatic Corporation. “SVS6 Electric Steam Boiler Specifications.”, 2004, Long Island City, New York.

12. Villescas, I., Flow field Surveys in a Transonic Compressor Prior to Inlet Steam Ingestion Tests, Master's Thesis, Naval Postgraduate School, Monterey, California, September 2005.

THIS PAGE INTENTIONALLY LEFT BLANK

APPENDIX A- CASE WALL SCHEMATIC

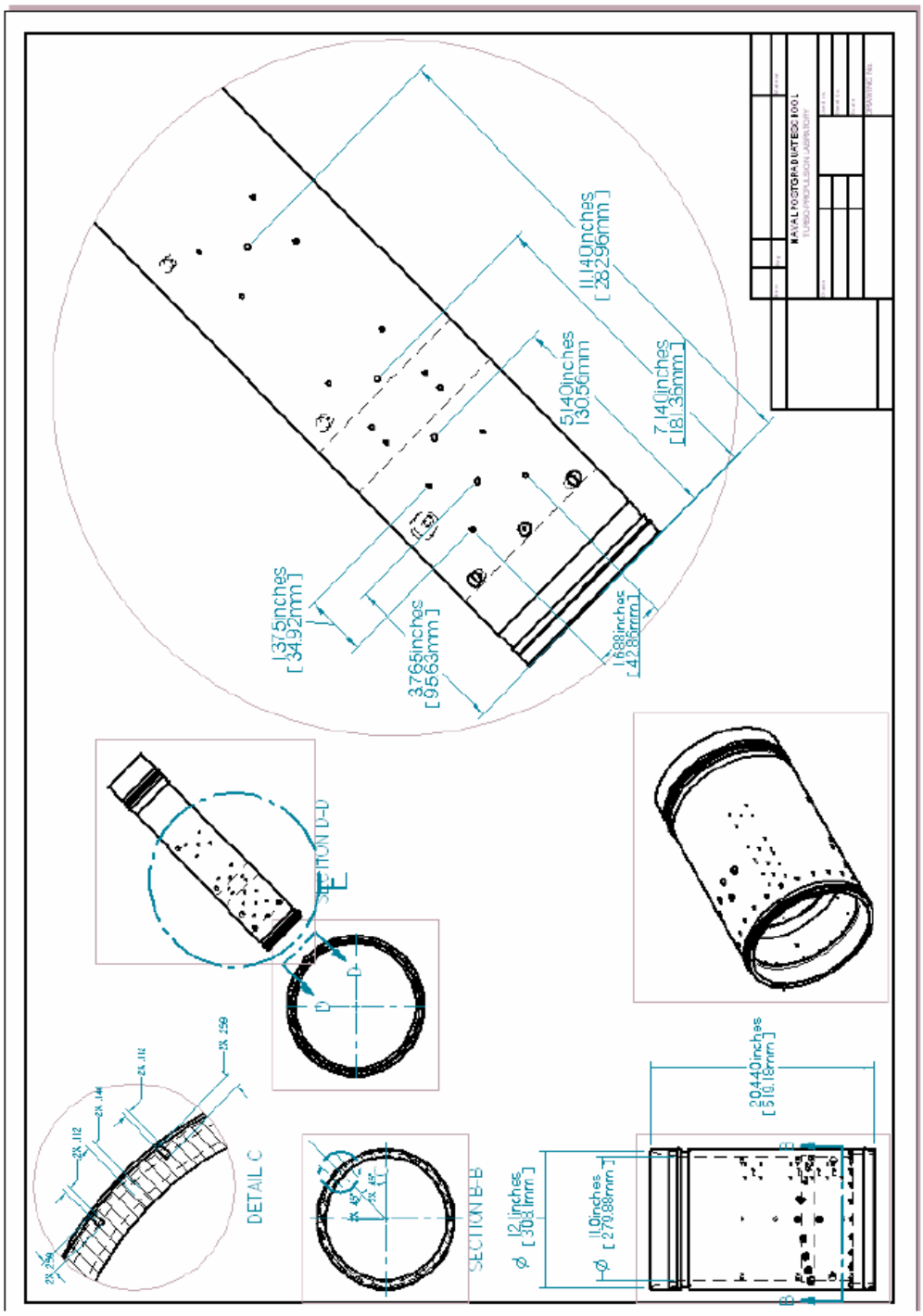

THIS PAGE INTENTIONALLY LEFT BLANK

APPENDIX B – FIVE HOLE PROBE UPSTREAM SURVEY RAW DATA

APPENDIX B-1 – 70% DESIGN SPEED OPEN THROTTLE

Position(m)	P1 [Pa]	P2 [Pa]	P3 [Pa]	P4 [Pa]	P5 [Pa]	Psj [Pa]	P0j [Pa]
0.110	97931.06	95116.73	94868.2	97284.62	97126.66	93597.35	98246.06
0.094	97948.05	94971.36	94687.45	97254.72	97084.32	93577.31	98258.65
0.080	97933.08	94791.47	94457.34	97215.52	97030.81	93567.09	98194.87
0.066	97953.72	94709.68	94260.92	97202.19	97020.83	93583.86	98196.9
0.054	97938.34	94609.25	94113.96	97103.6	96976.11	93521.28	98224.53
0.041	97921.34	94499.3	94008.31	96946.87	96981.7	93576.09	98214.78
0.031	97901.51	94298.12	93958.53	96971.51	96978.91	93556.45	98195.69
0.022	97906.37	94400.09	93981.6	96929.5	97006.46	93558.91	98154.66
0.014	97886.95	94585.03	94182.38	97060.78	96998.87	93629.67	98159.53
0.008	97900.71	94626.71	94215.17	97129.86	96965.33	93548.27	98186.75
0.004	97640.96	94465.97	94063.36	97033.71	96570.17	93529.87	98117.29
0.002	97114.52	94328.67	93685.82	96662.58	95974.7	93525.78	98094.14
0.001	97029.65	94231.48	93646.17	96657.74	95859.89	93565.04	98047.43

APPENDIX B-2 – 70% DESIGN SPEED PEAK EFFICIENCY

Position(m)	P1 [Pa]	P2 [Pa]	P3 [Pa]	P4 [Pa]	P5 [Pa]	Psj [Pa]	P0j [Pa]
0.109	94332.38	91904.44	91728.65	93734.7	93662.67	90579.02	95665.61
0.094	94352.5	91764.94	91536.76	93774.89	93616.99	90613.69	95328.34
0.080	94426.95	91762.96	91415.84	93797.8	93634.86	90627.15	95192.74
0.066	94362.16	91606.12	91215.99	93661.57	93571.71	90546.8	95067.68
0.054	94346.87	91520.8	91093.53	93609.33	93537.95	90545.99	94894.9
0.041	94311.46	91418.9	90969.88	93530.19	93514.12	90600.64	94833.41
0.032	94323.93	91287.02	90936.86	93532.2	93537.55	90534.98	94771.51
0.023	94293.36	91396.79	90935.25	93499.26	93533.19	90531.71	94774.75
0.014	94314.68	91590.32	91159.59	93539.83	93568.14	90555.37	94760.59
0.008	94282.49	91525.93	91184.16	93674.02	93495.46	90544.36	94727.82
0.004	94036.31	91431.54	90957.8	93466.32	93139.34	90513.77	94674.83
0.002	93651.55	91244.77	90792.72	93314.1	92709.26	90576.98	94682.11
0.001	93484.77	91187.92	90634.12	93133.81	92516.52	90471.36	94692.22

APPENDIX B-3 – 70% DESIGN SPEED NEAR STALL

Position(m)	P1 [Pa]	P2 [Pa]	P3 [Pa]	P4 [Pa]	P5 [Pa]	Psj [Pa]	P0j [Pa]
0.109	90551.23	88615.88	88441.05	90079.64	89991.45	87384.31	92819.91
0.094	90564.83	88530.19	88297.91	90091.22	89983.16	87428.23	92371.25
0.080	90586.83	88454.73	88179.26	90089.22	89969.73	87423.35	92028.06
0.066	90570.03	88356.09	88059.43	90028.9	89942.48	87492.48	91760.79
0.053	90544.83	88268.46	87926	89982.96	89889.57	87394.07	91558.88
0.041	90505.24	88183.6	87807.42	89898.68	89849.29	87325.76	91451.7
0.031	90593.62	88238.21	87863.9	89919.05	89961.04	87429.85	91272.83
0.022	90503.24	88140.79	87847.07	89863.53	89870.62	87312.75	91220.86
0.015	90429.27	88158.07	87893.14	89834.78	89833.89	87313.97	91106.48
0.009	90438.07	88242.93	87978.08	89935.83	89794.41	87406.27	91129.44
0.004	90278.15	88171.82	87845.07	89882.31	89574.15	87388.79	91038.42
0.002	89983.22	88055.55	87705.28	89716.18	89245.87	87454.25	91006.2
0.001	89831.81	88000.17	87661.23	89529.75	89082.59	87366.42	90994.53

APPENDIX B-4 – 90% DESIGN SPEED OPEN THROTTLE

Position(m)	P1 [Pa]	P2 [Pa]	P3 [Pa]	P4 [Pa]	P5 [Pa]	Psj [Pa]	P0j [Pa]
0.109	96017.77	91687.5	91472.67	95009.07	94805.3	89395.29	95157.93
0.094	95956.04	91422.85	91077.01	94924.12	94648.14	89370.44	95703.68
0.080	96008.49	91314.26	90788.29	94861.31	94640.18	89418.52	95824.38
0.066	95999.61	91024.51	90481.61	94715.59	94567.78	89406.29	95827.62
0.053	96000.42	90945.59	90350.45	94762.28	94560.62	89438.07	95952.38
0.041	95951.6	90698.61	90135.26	94561.46	94490.22	89337.04	96041.92
0.031	95954.43	90646.55	89963.98	94574.74	94541.53	89417.7	96065.82
0.022	95908.84	90564.51	90041.17	94548.59	94545.9	89377.37	96077.98
0.015	95964.11	90930.59	90321.48	94623.03	94647.34	89452.74	96231.55
0.008	95866.49	90893.5	90259.54	94706.34	94452.83	89440.92	96191.44
0.004	95508	90708.47	90013.02	94444.78	93919.32	89418.92	96277.35
0.001	94632.22	90393.38	89435.15	94065.52	92859.59	89372.07	96263.16
0.001	94526.76	90309.81	89434.34	94017.27	92783.03	89418.92	96237.23

APPENDIX B-5 – 90% DESIGN SPEED PEAK EFFICIENCY

Position(m)	P1 [Pa]	P2 [Pa]	P3 [Pa]	P4 [Pa]	P5 [Pa]	Psj [Pa]	P0j [Pa]
0.109	90399.68	86459.1	86261.66	89512.18	89282.95	84273.13	93595.96
0.095	90361.7	86226.06	85948.12	89413.2	89176.06	84127.6	92870.36
0.080	90446.46	86094.5	85716.17	89445.93	89181.97	84225.7	92427.72
0.066	90397.28	85905.04	85442.02	89295.08	89065.24	84303.13	92067.58
0.053	90303.34	85668.3	85180.36	89174.59	88991.5	84140.57	91531.08
0.041	90306.93	85601.41	85025.65	89092.82	88959.56	84220.43	91279.68
0.031	90347.31	85421.49	84990.17	89083.24	89059.32	84289.34	90807.3
0.022	90374.5	85503.62	85010.5	89113.96	89133.46	84273.13	91129.84
0.014	90195.01	85689.43	85043.99	88942.85	88986.77	84169.35	91076.27
0.008	90111.09	85684.34	85079.48	89058.11	88850.35	84175.03	90970.77
0.004	89838.2	85448.86	84916.43	89071.68	88381.81	84337.18	90888.63
0.002	89280.82	85245.92	84417.19	88611.15	87720.38	84160.84	90891.44
0.000	88643.42	85096.98	84588.47	88251.35	87085.98	84305.56	90900.7

APPENDIX B-6 – 90% DESIGN SPEED NEAR STALL

Position(m)	P1 [Pa]	P2 [Pa]	P3 [Pa]	P4 [Pa]	P5 [Pa]	Psj [Pa]	P0j [Pa]
0.110	83770.56	80555.86	80380.11	83082.38	82854.11	78457.51	86922.28
0.094	83743.27	80380.16	80078.42	83046.43	82771.34	78539.74	85905.19
0.080	83815.65	80291.35	79920.33	82943.35	82785.79	78622.39	85020.49
0.066	83702.54	80068.05	79586.49	82795.28	82622.23	78487.74	84697.56
0.054	83757.91	79982.39	79525.67	82832.4	82654.63	78516.77	84486.22
0.042	83767.79	79887.06	79430.9	82793.7	82675.32	78522.41	84395.54
0.031	83781.64	79878.15	79351.14	82714.35	82721.76	78488.95	84331.63
0.021	83690.29	79779.35	79339.7	82685.14	82672.97	78462.75	84258.15
0.014	83642.05	79861.48	79436.43	82659.88	82636.67	78482.5	84196.65
0.008	83714.8	80063.78	79627.96	82921.63	82659.7	78630.46	84167.9
0.005	83343.6	79828.94	79328.25	82636.59	82200.87	78508.7	84210.63
0.001	82747.16	79586.05	79023.95	82300.39	81554.95	78574.42	84209.83
0.001	82597.94	79533.77	79094.59	82199.41	81401.08	78576.43	84128.37

THIS PAGE INTENTIONALLY LEFT BLANK

APPENDIX C – THREE-HOLE PROBE UPSTREAM SURVEY RAW DATA

APPENDIX C-1 – 70% DESIGN SPEED OPEN THROTTLE

Position(m)	P1 [Pa]	P2 [Pa]	P3 [Pa]	Poj [Pa]	Psj [Pa]
0.139	95532.7	97282.23	95547.42	97156.67	92983.73
0.124	95127.52	97260.92	95888.3	97297.21	92973.57
0.109	95018.11	97232.07	95804.35	97322.3	92980.34
0.094	94893.73	97241.27	95699.63	97236.98	92979.49
0.079	94731.74	97246.29	95580.49	97276.71	92973.99
0.066	94679.17	97212.01	95485.52	97240.32	93009.13
0.052	94588.99	97204.48	95340.94	97197.24	92926.57
0.041	94561.63	97235.42	95346.03	97260.82	92950.7
0.031	94577.88	97220.37	95407.51	97227.78	92957.9
0.022	94633.01	97188.6	95438.46	97154.16	92966.37
0.014	94659.51	97184.84	95452.45	97252.04	92989.66
0.008	94660.37	97131.75	95444.82	97277.97	92915.56
0.004	94649.68	96931.11	95334.58	97254.55	92968.06
0.001	94391.95	96316.22	94964.45	97182.19	93003.63
0.000	94232.1	95986	94810.12	97210.21	92928.26

APPENDIX C-2 – 70% DESIGN SPEED PEAK EFFICIENCY

Position(m)	P1 [Pa]	P2 [Pa]	P3 [Pa]	Poj [Pa]	Psj [Pa]
0.140	91945.9	93694.07	92490.94	93727.31	89994.21
0.125	91775.8	93647.26	92480.34	93730.24	89973.04
0.109	91736.05	93691.98	92448.11	93805.11	89926.05
0.094	91586.46	93650.18	92339.57	93649.51	89992.52
0.079	91461.65	93619.25	92246.3	93590.95	89947.64
0.065	91450.97	93673.17	92181.43	93677.95	89987.44
0.053	91403.53	93665.65	92080.52	93680.88	89981.09
0.041	91378.31	93662.72	92089.42	93704.72	90003.95
0.030	91352.66	93642.24	92067.8	93665.82	89966.27
0.021	91391.56	93619.67	92083.91	93704.3	90014.96
0.014	91395.83	93605.46	92102.14	93724.8	89968.81
0.008	91406.94	93537.74	92084.76	93679.21	89966.27
0.004	91421.48	93378.06	92005.05	93673.77	90028.93
0.002	91312.06	93058.29	91827.83	93599.74	90046.29
0.001	91182.56	92733.91	91646.79	93625.25	90011.15

APPENDIX C-3 – 70% DESIGN SPEED NEAR STALL

Position(m)	P1 [Pa]	P2 [Pa]	P3 [Pa]	Poj [Pa]	Psj [Pa]
0.140	88525.79	89963.37	88977.82	90252.77	87012.74
0.124	88421.51	89981.76	89021.07	90154.06	86955.58
0.109	88364.23	89973.82	88960.86	90068.74	86971.67
0.094	88191.99	89902.76	88806.96	89962.08	86895.04
0.079	88151.39	89950.83	88793.39	89980.06	86917.05
0.066	88128.31	89952.09	88735.73	89902.27	86900.12
0.052	88110.78	89975.49	88685.27	89900.18	86910.7
0.041	88053.51	89955.85	88643.72	89949.95	87009.77
0.030	88048.81	89921.57	88641.18	89976.72	86991.57
0.022	88062.49	89902.34	88640.76	89943.68	86906.05
0.014	88009.91	89834.63	88575.46	89878.84	86879.37
0.008	88020.17	89789.48	88585.21	89856.68	86753.2
0.003	87952.64	89572.12	88400.36	89824.89	86713.83
0.000	87726.12	89072.18	88136.22	89785.15	86734.15
0.001	87776.12	89084.31	88177.77	89866.71	86827.72

APPENDIX C-4 – 90% DESIGN SPEED OPEN THROTTLE

Position(m)	P1 [Pa]	P2 [Pa]	P3 [Pa]	Poj [Pa]	Psj [Pa]
0.139	92701.99	95318.44	92682.15	95241.85	88726.6
0.124	92855	95344.78	92427.34	95326.34	88746.92
0.109	92768.66	95369.02	92251.81	95284.1	88759.62
0.094	92653.69	95394.94	92102.57	95412.08	88736.76
0.079	92484.44	95342.69	91871.5	95346	88708.39
0.066	92440.41	95326.39	91615.41	95256.91	88776.98
0.053	92405.37	95383.23	91457.69	95364.82	88746.92
0.041	92412.63	95378.64	91339.4	95355.62	88749.46
0.030	92454.09	95378.64	91412.33	95334.71	88773.59
0.022	92438.7	95306.74	91459.81	95344.74	88751.58
0.013	92404.51	95262.43	91476.77	95367.75	88738.88
0.008	92538.29	95239.02	91525.1	95406.65	88735.49
0.003	92298.09	94884.14	91512.38	95415.85	88799.84
0.001	91783.49	93973.3	91049.4	95380.71	88749.46
0.000	91539.44	93587.48	90922.63	95300.41	88776.98

APPENDIX C-5 – 90% DESIGN SPEED PEAK EFFICIENCY

Position(m)	P1 [Pa]	P2 [Pa]	P3 [Pa]	Poj [Pa]	Psj [Pa]
0.139	87450.44	89646.94	86968.15	89624.12	83568.08
0.125	87364.1	89639	86927.02	89583.97	83566.81
0.109	87353.85	89669.1	86868.94	89737.05	83747.6
0.094	87217.5	89700.03	86684.93	89668.88	83635.82
0.080	87117.49	89700.86	86539.5	89652.14	83805.18
0.065	87035.85	89694.18	86277.48	89599.44	83676.05
0.053	86969.18	89661.15	86080.33	89609.06	83617.2
0.041	86882.42	89593.44	85900.14	89550.09	83520.66
0.031	86954.65	89631.48	86004.01	89659.26	83634.98
0.022	87030.3	89623.95	86111.28	89738.31	83676.47
0.014	87033.29	89600.13	86160.89	89724.09	83768.77
0.008	87036.71	89531.15	86165.55	89580.62	83602.8
0.003	86846.51	89201.35	86076.94	89617.43	83663.77
0.001	86330.21	88343.6	85724.61	89586.9	83616.77
0.000	86110.09	87909.29	85581.3	89570.58	83531.67

APPENDIX C-6 – 90% DESIGN SPEED NEAR STALL

Position(m)	P1 [Pa]	P2 [Pa]	P3 [Pa]	Poj [Pa]	Psj [Pa]
0.139	80676.47	82546.28	80370.56	82762.05	77466.27
0.124	80370.02	82557.56	80653.78	82704.75	77551.79
0.109	80211.02	82510.33	80462.57	82626.11	77538.67
0.094	80117.42	82544.19	80387.95	82603.53	77632.66
0.080	79933.63	82474.38	80174.26	82470.94	77438.75
0.065	79836.19	82453.48	79963.97	82472.19	77439.17
0.053	79842.6	82477.73	79931.74	82485.16	77621.23
0.041	79800.71	82469.37	79871.96	82457.13	77479.82
0.030	79827.21	82490.68	79919.02	82547.48	77549.25
0.022	79849.44	82413.35	79927.08	82518.62	77471.77
0.014	79791.74	82372.39	79905.03	82412.38	77489.55
0.008	79875.08	82342.29	79927.93	82485.58	77439.17
0.003	79795.58	82035.89	79787.59	82454.21	77425.2
0.001	79455.79	81356.63	79530.23	82497.71	77516.23
0.000	79311.76	81066.54	79392.86	82416.56	77392.6

THIS PAGE INTENTIONALLY LEFT BLANK

APPENDIX D – FIVE HOLE PROBE DOWNSTREAM SURVEY RAW DATA

APPENDIX D-1 – 70% DESIGN SPEED OPEN THROTTLE

Position(m)	Angle(^{o})	P1 [Pa]	P2 [Pa]	P3 [Pa]	P4 [Pa]	P5 [Pa]	Psj [Pa]	P0j [Pa]
0.021	-22.5	110340.8	101156.6	99441.94	109998.3	108563.1	93726.93	98159.28
0.019	-22.4	110067.7	100987.8	99703.75	109744.1	108468.4	93726.52	98132.07
0.018	-22.3	109789.8	100992.2	99715.19	109328.6	108269.7	93729.8	98084.95
0.016	-22.4	109572.2	100859.1	100032.3	109173.8	108215.7	93773.57	98131.66
0.012	-22.5	109184.5	100667.1	100266.1	108690.8	107957	93722.84	98034.19
0.011	-22.4	108952.7	100661.9	100391.3	108414.9	107816.2	93690.94	98012.26
0.007	-22.4	108799.6	100737.7	100705.9	108244.7	107741.1	93720.8	98094.29
0.005	-22.4	108779	101006.6	100733.7	108215.6	107700.1	93734.3	98042.31
0.003	-23.2	108800.8	101143	100817.2	108430.9	107684.7	93678.26	98108.91
0.002	-25.8	108685.6	100644.7	101147.1	108653.8	107165.4	93653.31	97890.84
0.001	-25.9	108457.6	100670.3	100985	108449.4	106741.7	93742.89	98025.66
0.000	-25.9	107573.8	100962.1	100411.7	107774.7	105227	93783.79	98109.73

APPENDIX D-2 – 70% DESIGN SPEED PEAK EFFICIENCY

Position(m)	Angle(^{o}0	P1 [Pa]	P2 [Pa]	P3 [Pa]	P4 [Pa]	P5 [Pa]	Psj [Pa]	P0j [Pa]
0.022	-30.6	110083.4	99636.46	100004.1	109400.7	107954.6	90849.06	94741.46
0.020	-30.7	109780.8	99498.85	100235.5	109013.3	107816.2	90898.42	94780.7
0.018	-30.6	109554.5	99578.45	100441.6	108771.9	107762.2	90879.65	94793.24
0.015	-28.0	109270.2	100450.8	100043.7	108361.5	107693.6	90855.18	94785.96
0.011	-28.0	108845.3	100219.3	100387.2	107949.7	107414.8	90804.59	94817.91
0.007	-28.0	108729.6	100534.9	100687	107911.1	107475.7	90906.58	94733.37
0.005	-28.0	108770.4	100808.2	100717.3	108047.5	107525.2	90954.31	94722.45
0.003	-31.6	108848.2	100166.8	101521.9	108202	107418.1	90884.55	94738.22
0.002	-31.6	108564.2	100604.6	100937.5	108237.8	106757.5	90877.61	94737.41
0.002	-31.7	108551.4	100677.1	100866.7	108261.2	106755.9	90865.38	94708.29
0.000	-32.9	107593.1	100730	100452.2	107619.5	105079.4	90898.01	94870.51

APPENDIX D-3 – 70% DESIGN SPEED NEAR STALL

Position(m)	Angle(^{o})	P1 [Pa]	P2 [Pa]	P3 [Pa]	P4 [Pa]	P5 [Pa]	Psj [Pa]	P0j [Pa]
0.022	-39.5	109060.2	99322.07	99505.24	108085.7	106963.9	87205.95	91901.07
0.020	-39.4	108822.6	99327.67	99715.59	107822.4	106877.5	87229.53	91527.47
0.018	-38.6	108541.1	99722.89	99639.61	107523.4	106791.6	87341.74	90876.59
0.015	-38.6	108431.3	99697.28	100006.1	107369.9	106823.6	87276.28	90614.53
0.013	-38.6	108397.6	99739.29	100233.8	107343.2	106918.9	87264.49	90563.42
0.011	-37.5	108329.3	100051.9	100230.2	107248	106924.9	87315.31	90473.28
0.009	-37.6	108248.3	100185.2	100273.5	107175.4	106920.1	87319.78	90401.25
0.007	-37.6	108312.4	100417.5	100278.4	107148.7	106993.1	87281.57	90362.22
0.005	-37.7	108510.7	100797	100366.7	107405.6	107115.1	87304.74	90396.02
0.003	-40.6	108695.5	100665.5	100761.1	107755.4	107131.7	87238.47	90352.16
0.002	-43.5	108314.1	100558.9	100750	107598.1	106522.1	87322.63	90441.49
0.001	-43.5	108101.9	100835.9	100449.3	107465.5	106248.3	87321.82	90398.03
0.000	-47.8	107390.1	100459.6	100606.8	107229.9	105150.2	87322.63	90427.4

APPENDIX E- THREE-HOLE PROBE OPEN THROTTLE CORRECTED MASS FLOW RATES

APPENDIX E-1 70% DESIGN SPEED NEW INLET HONEYCOMB

Position(m)	Tp (K)	Mach_m	T (K)	u (m/s)	P2 [Pa]	Ps [Pa]	ρ (kg/m^3)	dr (m)	r (m)	u(m/s)	m(kg/s)
0.139	288.8	0.220	286.0	74.67	97282.2	93992.7	1.15	0.015	0.132	75.33	1.07
0.124	288.8	0.223	285.9	75.98	97260.9	93856.8	1.14	0.015	0.117	76.76	0.99
0.109	288.8	0.228	285.8	77.53	97232.1	93690.7	1.14	0.015	0.101	78.88	0.86
0.094	288.8	0.236	285.5	80.22	97241.3	93453.1	1.14	0.014	0.087	81.77	0.73
0.079	288.8	0.245	285.3	83.31	97246.3	93165.0	1.14	0.014	0.073	83.46	0.59
0.066	288.8	0.246	285.3	83.61	97212.0	93103.0	1.14	0.014	0.059	84.15	0.49
0.052	288.8	0.249	285.2	84.69	97204.5	92991.3	1.14	0.011	0.046	85.11	0.31
0.041	288.8	0.252	285.1	85.53	97235.4	92938.3	1.14	0.010	0.036	85.51	0.22
0.031	288.8	0.252	285.1	85.49	97220.4	92927.3	1.14	0.009	0.026	84.76	0.15
0.022	288.8	0.247	285.2	84.02	97188.6	93041.5	1.14	0.008	0.018	83.68	0.08
0.014	288.8	0.245	285.3	83.35	97184.8	93102.9	1.14	0.006	0.011	82.98	0.04
0.008	288.8	0.243	285.3	82.61	97131.8	93122.9	1.14	0.004	0.006	80.66	0.01
0.004	288.8	0.232	285.7	78.71	96931.1	93294.2	1.14	0.003	0.002	75.51	0.00
0.001	288.8	0.213	286.2	72.31	96316.2	93259.5	1.14	0.001	0.000	70.96	0.00
0.000	288.8	0.205	286.3	69.61	95986.0	93160.5	1.13				
mdot_tot (kg/s)	5.55	mdot_corr (kg/s)	5.99								

APPENDIX E-2 70% DESIGN SPEED OLD INLET HONEYCOMB

Position(m)	Tp (K)	Mach_m	T (k)	u (m/s)	P2 [Pa]	Ps [Pa]	ρ (kg/m^3)	dr (m)	r (m)	u(m/s)	m
0.13992	288.4	0.217267	285.6	73.867	96981.92	93767.5	1.144	0.0156	0.1321	74.395	1.105
0.12429	288.4	0.220405	285.6	74.923	96973.64	93668	1.143	0.0154	0.1166	79.587	1.028
0.10885	288.4	0.24817	284.8	84.251	96976.13	92809.8	1.135	0.015	0.1014	85.122	0.921
0.09389	288.4	0.253368	284.7	85.992	96956.66	92619.9	1.134	0.0147	0.0865	86.902	0.789
0.07916	288.4	0.258802	284.5	87.812	96962.46	92443.1	1.132	0.0135	0.0724	88.633	0.615
0.06568	288.4	0.263707	284.3	89.453	96983.99	92296.1	1.131	0.0132	0.0591	90.172	0.501
0.05244	288.4	0.268009	284.2	90.892	96969.5	92133.2	1.13	0.0113	0.0468	91.127	0.342
0.04114	288.4	0.269416	284.2	91.362	96991.86	92105.2	1.129	0.0107	0.0358	91.087	0.248
0.03039	288.4	0.267772	284.2	90.812	96963.29	92135.5	1.13	0.009	0.0259	91.871	0.152
0.0214	288.4	0.274112	284.0	92.93	96931.4	91881.8	1.127	0.0078	0.0175	91.171	0.088
0.01363	288.4	0.263581	284.4	89.411	96911.11	92231.1	1.13	0.0059	0.0107	86.16	0.039
0.00771	288.4	0.244167	284.9	82.908	96797.63	92768.4	1.134	0.0042	0.0056	82.369	0.014
0.0035	288.4	0.240953	285.0	81.83	96107.68	92209	1.127	0.0028	0.0021	68.748	0.003
0.00066	288.4	0.163394	286.8	55.667	94747.23	92954.4	1.129	0.0002	0.0006	41.65	3E-05
0.00045	288.4	0.080944	288.0	27.634	94160.81	93719.5	1.134				
mdot_tot (kg/s)	5.84	mdot_corr (kg/s)	6.32								

APPENDIX E-3 90% DESIGN SPEED NEW INLET HONEYCOMB

Position (m)	Tp (K)	Mach_m	T (k)	u (m/s)	P2(kg/m^3)	Ps(kg/m^3)	ρ (kg/m^3)	dr	r	u(m/s)	m (kg/s)
0.13907	294	0.2755	289.5	94.296	95318.44	90304.2	1.087	0.0147	0.1317	95.037	1.259
0.12434	294	0.2799	289.4	95.778	95344.78	90173.4	1.086	0.0152	0.1167	97.108	1.174
0.10916	294	0.2878	289.1	98.437	95369.02	89911.2	1.084	0.0154	0.1014	99.748	1.064
0.09372	294	0.2956	288.8	101.06	95394.94	89647.5	1.081	0.0144	0.0865	102.28	0.868
0.07927	294	0.3029	288.6	103.51	95342.69	89323	1.079	0.0137	0.0724	104.61	0.705
0.06554	294	0.3095	288.3	105.72	95326.39	89054	1.076	0.0127	0.0592	106.96	0.545
0.05281	294	0.3169	288.1	108.2	95383.23	88817.1	1.074	0.012	0.0468	108.63	0.412
0.04079	294	0.3195	288	109.07	95378.64	88709.6	1.073	0.0109	0.0354	108.62	0.281
0.02993	294	0.3168	288.1	108.17	95378.64	88816.8	1.074	0.0084	0.0257	107.46	0.157
0.02151	294	0.3126	288.2	106.76	95306.74	88915	1.075	0.0083	0.0174	106.47	0.103
0.01323	294	0.3109	288.3	106.19	95262.43	88939.9	1.075	0.0055	0.0105	105.3	0.041
0.00774	294	0.3056	288.5	104.41	95239.02	89122.8	1.076	0.0044	0.0055	102.55	0.017
0.00329	294	0.2945	288.9	100.69	94884.14	89208.3	1.076	0.0027	0.0019	97.206	0.003
0.00057	294	0.2738	289.6	93.723	93973.3	89088.6	1.072	0.0006	0.0003	91.952	1.00E-04
1.60E-05	294	0.2633	289.9	90.18	93587.48	89077.3	1.071				
mdot_tot(kg/s)	6.63	mdot_corr (kg/s)	7.52								

APPENDIX E-4 90% DESIGN SPEED OLD INLET HONEYCOMB

Position (m)	Tp (K)	Mach_m	T (k)	u (m/s)	P2 [Pa]	Ps [Pa]	P(kg/m^3)	dr(m)	r (m)	u(m/s)	m (kg/s)
0.139	298.8	0.309	293.1	106.43	94955.54	88724.9	1.055	0.0156	0.1322	105.94	1.451
0.124	298.8	0.306	293.2	105.44	94959.27	88840.5	1.056	0.0156	0.1166	107.35	1.295
0.108	298.8	0.317	292.8	109.25	94965.06	88408.1	1.052	0.0151	0.1012	110.45	1.117
0.093	298.8	0.3244	292.5	111.66	94960.51	88118.9	1.05	0.0144	0.0864	113.64	0.931
0.079	298.8	0.336	292	115.62	94899.22	87582.5	1.045	0.0138	0.0724	116.3	0.761
0.065	298.8	0.340	291.9	116.98	94950.98	87462.2	1.044	0.0129	0.059	117.95	0.591
0.052	298.8	0.346	291.6	118.93	94927.79	87196.2	1.042	0.0118	0.0467	119.76	0.431
0.040	298.8	0.351	291.4	120.59	94917.02	86975.8	1.04	0.0104	0.0356	121.13	0.292
0.03038	298.8	0.354	291.3	121.67	94893	86815.3	1.038	0.0092	0.0258	120.5	0.187
0.021	298.8	0.347	291.6	119.33	94883.89	87105.8	1.041	0.0075	0.0174	114.75	0.098
0.013	298.8	0.320	292.7	110.18	94844.14	88186.5	1.05	0.0058	0.0107	108.87	0.045
0.007	298.8	0.312	292.9	107.56	94636.24	88296.8	1.05	0.0042	0.0056	107.08	0.017
0.003	298.8	0.309	293	106.59	93404.17	87257	1.037	0.0029	0.0021	68.978	0.003
0.0006	298.8	0.090	298.3	31.364	90065.38	89540.8	1.046	0.0009	0.0002	19.856	2E-05
-0.0003	298.8	0.024	298.8	8.348	89034.17	88997.4	1.038				
mdot_tot (kg/s)	7.22	mdot_corr (kg/s)	8.40								

INITIAL DISTRIBUTION LIST

1. Defense Technical Information Center
   Ft. Belvoir, VA

2. Dudley Knox Library
   Naval Postgraduate School
   Monterey, CA

3. Distinguished Professor and Chairman Anthony Healey
   Department of Mechanical and Aeronautical Engineering
   Naval Postgraduate School
   Monterey, CA

4. Professor Ray Shreeve
   Department of Mechanical and Aeronautical Engineering
   Naval Postgraduate School
   Monterey, CA

5. Professor Garth Hobson
   Department of Mechanical and Aeronautical Engineering
   Naval Postgraduate School
   Monterey, CA

6. Dr. Anthony Gannon
   Department of Mechanical and Aeronautical Engineering
   Naval Postgraduate School
   Monterey, CA

7. ENS Christopher W. Rose
   Monterey, CA